1987

High resolution-sensitivity charcterization of polycyclic aromatic hydrocarbon-DNA adducts using fluorescence line narrowing spectrometry

Richard Scott Cooper
Iowa State University

Order Number 8805058

High resolution-sensitivity characterization of polycyclic aromatic hydrocarbon-DNA adducts using fluorescence line narrowing spectrometry

Cooper, Richard Scott, Ph.D.

Iowa State University, 1987

U·M·I
300 N. Zeeb Rd.
Ann Arbor, MI 48106

PLEASE NOTE:

In all cases this material has been filmed in the best possible way from the available copy. Problems encountered with this document have been identified here with a check mark __✓__.

1. Glossy photographs or pages _____
2. Colored illustrations, paper or print _____
3. Photographs with dark background _____
4. Illustrations are poor copy _____
5. Pages with black marks, not original copy _____
6. Print shows through as there is text on both sides of page _____
7. Indistinct, broken or small print on several pages ✓
8. Print exceeds margin requirements _____
9. Tightly bound copy with print lost in spine _____
10. Computer printout pages with indistinct print _____
11. Page(s) _____ lacking when material received, and not available from school or author.
12. Page(s) _____ seem to be missing in numbering only as text follows.
13. Two pages numbered _____. Text follows.
14. Curling and wrinkled pages _____
15. Dissertation contains pages with print at a slant, filmed as received ✓
16. Other _____

_____

_____

High resolution-sensitivity characterization of polycyclic aromatic hydrocarbon-DNA adducts using fluorescence line narrowing spectrometry

by

Richard Scott Cooper

A Dissertation Submitted to the
Graduate Faculty in Partial Fulfillment of the
Requirements for the Degree of
DOCTOR OF PHILOSOPHY

Department: Chemistry
Major: Analytical Chemistry

Approved:

Signature was redacted for privacy.
In Charge of Major Work

Signature was redacted for privacy.
For the Major Department

Signature was redacted for privacy.
For the Graduate College

Iowa State University
Ames, Iowa

1987

TABLE OF CONTENTS

I. INTRODUCTION

A. Cancer

Cancer has long been a menace and even after decades of intense research, much is unknown about this dread disease. It has been estimated that one out of every four people in the United States will develop cancer, and of these, 68% will die from cancer (1). For this reason, massive efforts are still directed towards the understanding of this disease.

Cancer is the autonomous growth and reproduction of cells. In other words, when a normal cell is transformed into a cancer cell, it obtains the ability to determine its own activity and retains its ability to produce transformed offspring. In the normal cell cycle, there is a block point that is used to regulate the initiation of the growth and reproductive processes. This block can be removed at the appropriate time by the addition of a specific stimulus or the removal of inhibitors (2). In a cancer cell, this block is either ignored or has been removed. Many researchers believe that this arises from a faulty DNA replication process that fails to provide the information necessary for cell regulation (2,3). Certain compounds have been implicated in this "faulty DNA replication process" and are known as chemical carcinogens.

One class of chemical carcinogens that has received a great deal of scientific attention is the polycyclic aromatic hydrocarbons (PAH). This interest in PAH as chemical carcinogens originated in 1775 when an alarmingly high incidence of scrotal cancer was observed in chimney sweeps (4). The offending agent was believed to be present in the soot to which these workers were continually exposed, and was finally isolated and identified as benzo[a]pyrene (B[a]P) (5). Since then many other PAH have been implicated in chemical carcinogenesis and mutagenesis (6-8). These compounds are of great interest since they are produced by the pyrolysis or the incomplete combustion of organic materials (9), and are, therefore, present virtually everywhere (10-12). Some common sources of PAH are industrial smoke stacks, motor vehicles, cigarettes, fireplaces, and charcoal grills.

Many researchers believe that the formation of an adduct between the genetic material DNA and carcinogens, including many of the PAH, is the crucial step in the initiation of carcinogenesis (13-15). It is interesting to note, however, that B[a]P and many other chemical carcinogens, by themselves, are not reactive towards DNA. Instead, they must be metabolized to some ultimate carcinogenic form that can then bind to DNA (16). Once a carcinogen has been

introduced into a cell it has many metabolic pathways it can follow.

As Figure 1 shows, a carcinogen must be metabolized to its ultimate carcinogenic form, which can attack the DNA in a susceptible cell to produce a "transformed cell." When this "transformed cell" reproduces it creates two daughter cells with the same defect as the original cell and the cancer process is initiated. It should be pointed out that there are several paths leading away from cancer. As an example, the carcinogen can be metabolized into an inactive metabolite that can be removed from the cell as waste. Also, many carcinogens are cell-type specific so that even in the presence of carcinogens some cells will not develop into tumor forming cells (17). Even the transformation of a susceptible cell does not guarantee tumor growth due to the presence of repair mechanisms that can repair damaged DNA (17-19). Also, if the carcinogen binds to the wrong portion of the DNA chain it may not affect the growth and reproduction of the cell. On the other hand, it could kill the cell, terminating the cancer process (17). Complicating the matter further, there are synergistic and antagonistic effects to take into account, where a second chemical compound either helps to facilitate or hinders the formation of DNA adducts (15).

Figure 1. General outline of the metabolic pathways available for a carcinogen

Figure 1

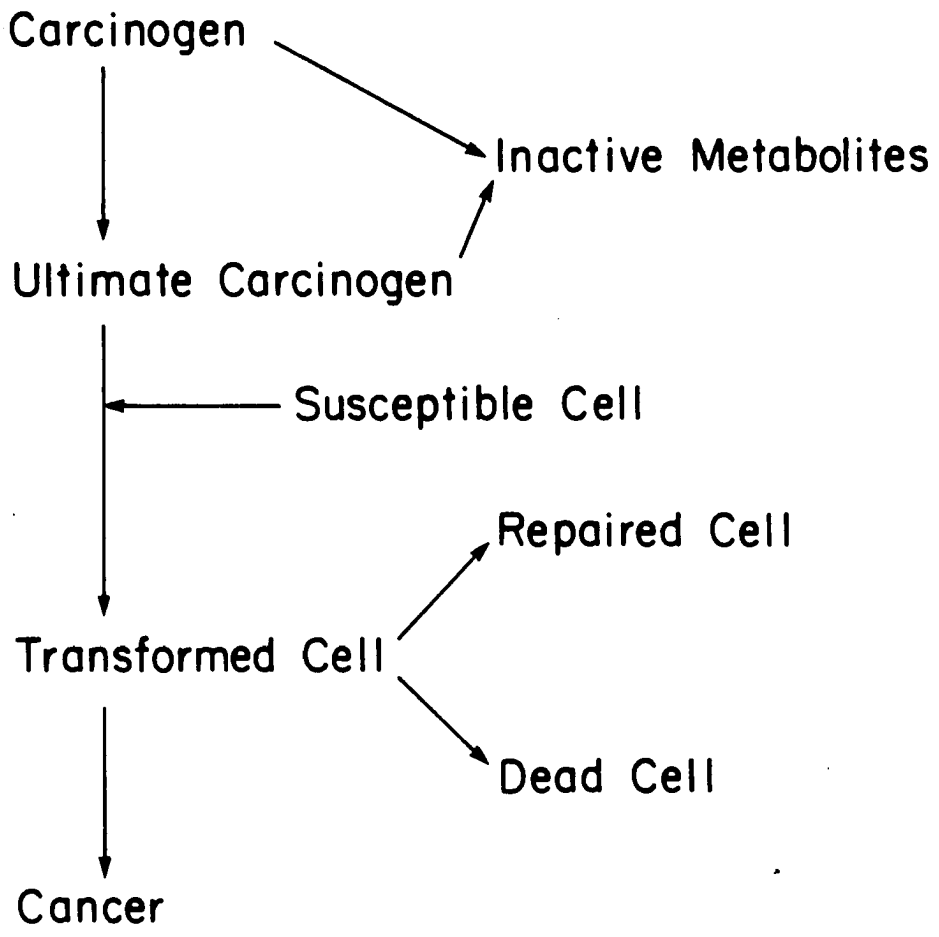
Carcinogen
Inactive Metabolites
Ultimate Carcinogen
Susceptible Cell
Repaired Cell
Transformed Cell
Dead Cell
Cancer

Truly it is a complicated process that leads from carcinogen exposure to cancer.

B. Metabolic Pathways

As was pointed out earlier, the important step in this process is believed to be the formation of DNA adducts. There have been several theories proposed to account for the formation of PAH-DNA adducts (20-23). Of these, the most widely held is the bay region theory (22). Following the hypothesis that many PAHs become carcinogens only after metabolic activation, much research was directed towards finding the ultimate carcinogenic forms of these PAH. In 1976, through the efforts of many researchers (24-28), strong evidence was obtained indicating that a diol epoxide formed from benzo[a]pyrene, trans-7,8-dihydroxy-anti-9,10-epoxy-7,8,9,10-tetrahydrobenzo[a]pyrene (BPDE), was an important carcinogenic form. This compound is formed, as shown in Figure 2, by monooxygenation followed hydrolysis and a second monooxygenation step. With this evidence and by interpreting substituent effects upon the carcinogenicity of benz[a]anthracene derivatives, Jerina and Daly postulated that it was the presence of a "bay region" that was the critical feature in benzo[a]pyrene and other PAH carcinogenesis (22). The prototype of a "bay region" in a PAH is the sterically hindered region of phenanthrene. The "bay region" of benzo[a]pyrene is indicated in Figure 2.

Figure 2. The bay region route of metabolism to form the diol epoxide of benzo[a]pyrene (22)

Figure 2

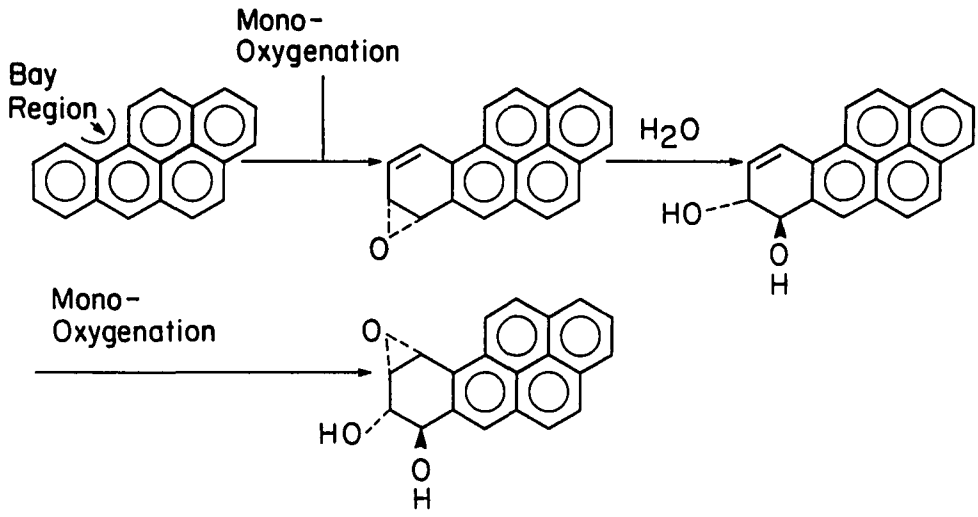
Mono-
Oxygenation
Bay
Region
H_2O
HO
O
H
Mono-
Oxygenation
O
HO
O
H

Quantum chemical calculations were used to estimate the ease of ring opening of the benzylic C-O epoxide bond to form a resonance stabilized carbocation and provided a theoretical basis for the bay region theory (29,30). The precise mechanism by which diol epoxides react with DNA is as yet unknown; however, for benzo[a]pyrene the major adduct is believed to occur at the N-2 position of guanine through the C-10 position of the benzo[a]pyrene, as shown in Figure 3 (31).

A second metabolic pathway has been proposed, and is known as "one electron oxidation" (20,21,32). By this mechanism PAH are oxidized to radical cations which can react with DNA. A PAH must possess two properties in order to be activated via this mechanism. First, in biological systems there are agents present that can oxidize compounds with an ionization potential less than 7.35 eV; therefore, the PAH ionization potential must be less than this to become a radical cation. Secondly, the radical cation formed must have its charge localized mainly on one carbon atom. If the charge is delocalized over many carbon atoms, no one carbon atom will possess enough electrophilicity to react with DNA (21). Benzo[a]pyrene meets both of these requirements and can form a radical cation with the charge localized mainly at the C-6 position (33). In vitro studies have indicated that this radical cation is indeed formed and

Figure 3. BPDE-DNA adduct with binding of the B[a]P derivative occurring at the C-10 position of the diol epoxide to the N-2 exocyclic nitrogen of guanine

Figure 3

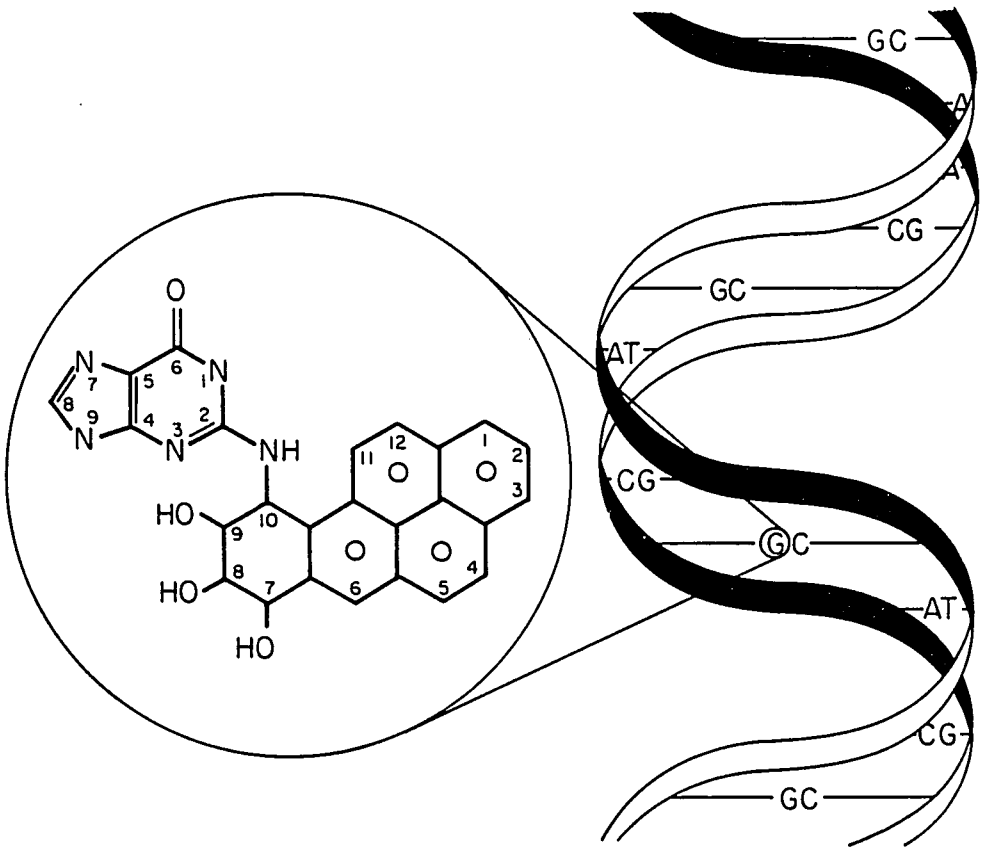

that it reacts mainly with the guanine base in DNA at the N-7 and C-8 positions (32). It should be pointed out that the adducts formed are unstable resulting in the depurination of these adducts (32). Some researchers believe that this cleavage of the adducts from the DNA is, at least in part, responsible for the initiation of the cancer process.

It is clear from the above discussions that in vivo identification of the DNA adducts is necessary to identify the metabolic pathways responsible for DNA damage. Detailed studies of competing metabolic activation pathways and subsequent reactions with DNA bases have been hampered by the unavailability of rapid methodologies for determination and characterization of the reactive intermediates and adducts. The availability of such methodologies would also be valuable for the study of DNA repair and synergistic and antagonistic effects associated with the components of mixtures of carcinogens and mutagens.

The attributes of an ideal method for the study of DNA damage are outlined here. First, high sensitivity is necessary so that the method is applicable to small samples of DNA with the low adduction levels found in real samples (31). The small DNA sample requirement emerges from the fact that one gram of tissue yields 1 mg of DNA and if samples from live humans are to be tested only small amounts

of tissue will be available. Second, high selectivity is necessary to resolve the complex mixtures found in real samples. Third, minimal sample preparation, the ability to examine intact DNA adducts, and short analysis time are all desirable to prevent undetectable changes in the sample leading to erroneous results and to facilitate the rapid routine analyses of samples. Fourth and last, broad applicability is needed for studies involving many different types of carcinogens.

C. Literature Review

Recent attempts at identifying DNA-PAH adducts have led to the development of several analysis techniques. The detection of DNA adducts long before clinical symptoms are apparent could be the basis for preventative methodologies. In Table 1 are listed several current approaches along with some figures of merit.

Of the various immunoassay techniques available for the study of DNA damage, enzyme-linked immunosorbent assay (ELISA) (13,31,34-38) is the most commonly employed. In this method a tailor made antibody, with one or more enzymes attached to it, is used to specifically bind to one type of DNA adduct. The DNA to be investigated is dried onto the walls of a sample well and exposed to the labeled antibody. Unreacted antibodies are removed with several washings and finally an enzyme substrate is added and allowed to react

Table 1. DNA-adduct detection methods (34)

Technique	Analyze	Amount of DNA (µg)	Detection Limit Adducts/base pair
ELISA	intact DNA	50	$1/10^8$
^{32}P-Postlabeling	base/adduct	5	$1/10^{10}$
GC/ECD	tetrols	500	$1/10^{10}$
GC/MS	tetrols	500	$1/10^9$
MS/MS	base/adduct	500	$1/10^9$
Synchronous Fluorescence	tetrols	100	$1/10^7$
HPLC/Fluorescence	tetrols	100	$1/10^7$
FLNS	intact DNA	20	$1/10^8$

for a predetermined period of time. The enzyme substrate reacts with the enzymes still present in the well to give a product whose concentration is easily determined by some physical method, e.g., colorimetry. With the knowledge of the reaction kinetics, reaction time, initial substrate concentration, and amount of DNA present, the damage level of the DNA, due to the specific adduct being determined, is easily calculated (35). The sensitivity of this method is good as defined by a damage level of ~ $1:10^8$ base pairs for ~ 50 µg of DNA. Prospects for improved sensitivity are centered on the use of even larger amounts of DNA (34). ELISA is applied to intact DNA and possesses a superior selectivity. However, an antibody must be developed and characterized for each and every adduct of interest. Furthermore, the immunoassays are likely to encounter difficulties for samples derived from cells which have been exposed to complex mixtures of genotoxic agents.

A second methodology is based on ^{32}P postlabeling (13,31,34,39-43). The use of ^{32}P postlabeling in the study of carcinogenic DNA adducts was first reported by Reddy et al. (43). This approach involves denaturation and hydrolysis of DNA to nucleoside monophosphates which are subsequently labeled with [^{32}P] phosphate, forming nucleoside biphosphates. The adducted along with the nonadducted or normal, labeled nucleotides are applied as a

spot to a thin layer chromatographic plate. The plate is developed in four dimensions, two to remove impurities, normal nucleotides, and phosphate groups, and two dimensions to resolve different adducts into separate spots on the chromatographic plate. Detection is performed autoradiographically. Identification of a spot is accomplished by comparing its position on the plate to that of standard adducts previously chromatographed. The sensitivity attainable is the highest currently available with detection limits in the attomole range (~ $1:10^{10}$ base pairs for 5 µg DNA) possible (41). ^{32}P-postlabeling also has the advantage of being generally applicable. The limitations of the technique include the use of radioactive ^{32}P, the limited resolving power of thin layer chromatography, and a 20-80 hour analysis time per sample.

Gas chromatography with electron-capture detector (GC/ECD) and gas chromatography/mass spectrometry (GC/MS) are also being applied to DNA damage analysis (13,34,44-46). Due to the nature of these techniques the DNA samples must be hydrolyzed and derivatized for increased volatility, thermal stability, and detectability (44-46). Since only the hydrolyzed products are expected to pass through a GC, structural information studies of base adducts and nucleotide adducts are not possible (34). To overcome this problem soft ionization sputter techniques for the high

polarity, thermally and chemically labile modified nucleotides are also being explored as alternate sample introduction methods for MS analysis, e.g., secondary ion mass spectrometry (SIMS) and fast atom bombardment (FAB) (13,47-51). However, significant improvements in mass range at highest sensitivity are required before soft ionization sputter techniques can be adequately exploited (34). The circumvention of derivatization is desirable because it is time consuming and can lead to uncertainties in quantitation.

Several fluorescence based techniques have also been utilized. Synchronous fluorescence spectroscopy (13,31,34, 52-56), in which the excitation and emission frequencies are scanned together to maintain a constant energy or wavelength difference between them, takes advantage of the sensitivity of fluorescence detection to allow the measurement of a single adduct in at least 10^8 DNA bases, for 100 µg of DNA (34). However, the line widths of the measured fluorescence bands are too broad to allow the distinction between chromophores that have severely overlapped $S^1 \leftarrow S_0$ absorption origins (31). In a second approach, which relies on fluorescence detection (31,34,57-60), DNA adducts are hydrolyzed to release the carcinogen moiety (in the case of benzo[a]pyrene, as free tetrols), and these are then extracted from the residual DNA and separated by high

performance liquid chromatography (HPLC). A modification level of ~ 1 adduct in 10^8 DNA bases, for a DNA sample of 100 µg, has been detected (34).

A final fluorescence based approach which affords high selectivity and can be applied to intact DNA adducts is fluorescence line narrowing spectrometry (FLNS) (61). Using this method, carcinogenic metabolites and/or DNA adducts are directly incorporated into a low temperature amorphous host. These matrices can be widely varied in composition in order to solubilize most any sample. Analyses are accomplished by exciting the low temperature (< 30 K) samples with a spectrally narrow line source, e.g., laser, and detecting the fluorescence. The fluorescence emitted, unlike room temperature fluorescence, is a pattern of spectrally narrow lines characteristic of the chromophore being excited and thus acts as an identifying "fingerprint." The fact that different chromophores yield different patterns and that the lines in these patterns are very narrow gives FLNS its high selectivity. It is the intent of this dissertation to show that FLNS is a rapid, broadly applicable, sensitive, and selective technique for the study of chemical carcinogenesis.

D. Theory: Principles of FLNS

The theory of FLNS has previously been discussed in great detail (62-65); therefore, only a brief discussion will be given here.

A solution containing PAH at room temperature possesses a broad absorption profile. Excitation of this solution yields an equally broad fluorescence profile. If, however, this solution were frozen to a low temperature (< 30 K) amorphous solid (glass), the homogeneous absorption linewidths for the individual PAH would be reduced. However, glasses are structurally disordered and therefore each molecule would occupy an energetically inequivalent site (62-65). Since the $S_1 \leftarrow S_0$ transition energy of a molecule is influenced by its environment, a distribution of narrow homogeneous absorption bands is formed and again yields a broad absorption profile known as a site inhomogeneously broadened absorption profile (62-65).

FLN is a site excitation energy (isochromat) selective spectroscopy which can eliminate or significantly reduce the contribution of site inhomogeneous line broadening, Γ_I, to spectral profiles (62-65). A site inhomogeneously broadened absorption profile is depicted in Figure 4 and is the convolution of a very large number of individual site absorptions possessing a homogeneous linewidth Γ. At liquid helium temperatures $\Gamma \lesssim 0.1$ cm^{-1}, while for amorphous molecular hosts such as glasses or polymers $\Gamma_I \sim 300\text{-}500$ cm^{-1}. Classical broad band excitation of all the energetically inequivalent sites which contribute to the profile of Figure 4 results in an equally broad fluorescence

Figure 4. Low temperature absorption profile of a solute in an amorphous solid. The inhomogeneous and homogeneous bandwidths (Γ_I and Γ) are indicated

Figure 4

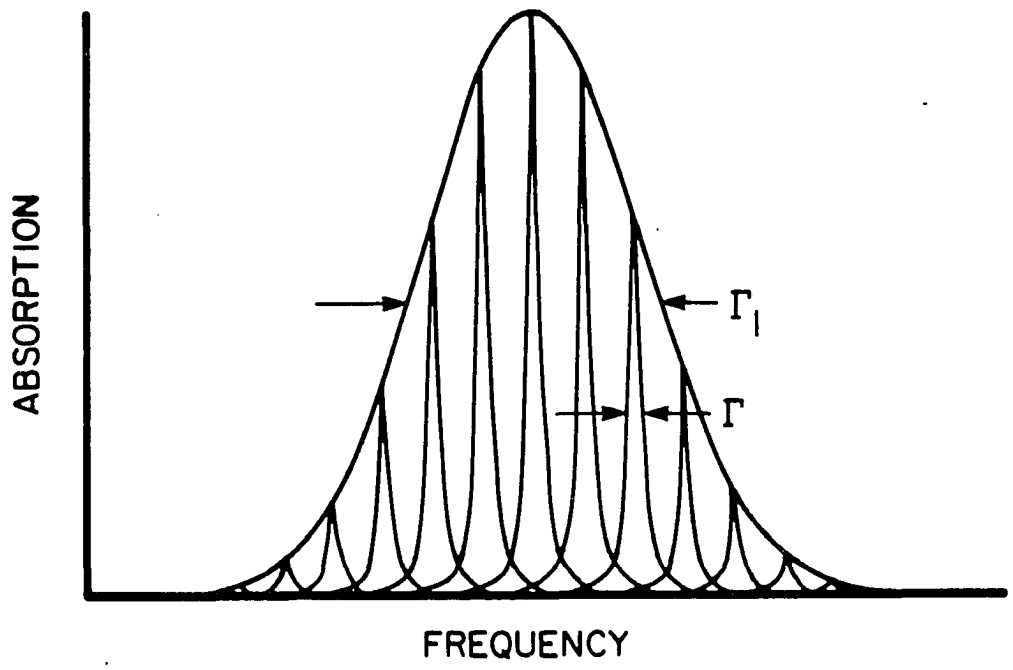

spectrum. Such spectral resolution does not allow for the distinction between substitutional isomers of a given PAH (for example) since their S_1 states typically lie within several tens of cm^{-1} from each other. However, selection of a narrow isochromat of the absorption profile with a laser of width $\Delta\nu << \Gamma_I$ can result in dramatic line narrowing provided certain conditions are met. First, the impurity concentration must be sufficiently low to preclude site randomization due to intermolecular energy transfer on a time scale comparable to the excited state lifetime. In addition, the fluorescence observed must originate from the electronic state being excited -- a consequence of the fact that site energy distribution functions for different electronic states are generally not correlated. Thus, the narrow isochromat of the state selected by the laser maps onto a much broader "polychromat" in another excited electronic state.

For practical applications of FLN on molecular systems, the origin or low lying vibronic transitions of the lowest excited singlet (S_1) state are generally excited. For origin excitation, the resonance fluorescence (origin) transition occurs at the laser frequency and is, therefore, not a reliable analytical line. Furthermore, the vibronic transitions provide only the ground state vibrational frequencies. Utilization of vibronic excitation is

significantly better from the standpoints of characterization and selectivity. Figure 5 depicts an absorption spectrum in which there are two overlapping vibronic transitions to fundamental excited state vibrations 1_α and 1_β. To the left is an energy level diagram in which the slanted parallel lines indicate the site inhomogeneous broadening for the $(1_\alpha,0)$ and $(1_\beta,0)$ transitions. The laser excitation frequency (ω_L) is chosen to excite different isochromats belonging to the $v'_\alpha = 1$ and $v'_\beta = 1$ levels. For example, ω_L selects an isochromat associated with $v'_\beta = 1$ that lies near the bottom of its distribution while that associated with $v'_\alpha = 1$ lies near the top of its distribution. As vibrational relaxation occurs on the picosecond timescale, it precedes the fluorescence which originates from the zero-point vibrational level. Vibrational relaxation is indicated by the downward wiggly arrows which show that fluorescence originates from two different isochromats that are linked to the two vibrations initially excited. The resulting fluorescence spectrum has the appearance of Figure 5b in which the laser line (ω_L) lies to higher energy of all fluorescence bands. Fluorescence from the two isochromats results in a doubling of the origin or (0,0.) transition as well as the (0,1) vibronic transitions. An important point is that the displacements between ω_L and the (0,0) bands provide the

Figure 5. Schematic representation of laser site selection in FLNS (see explanation in text)

Figure 5

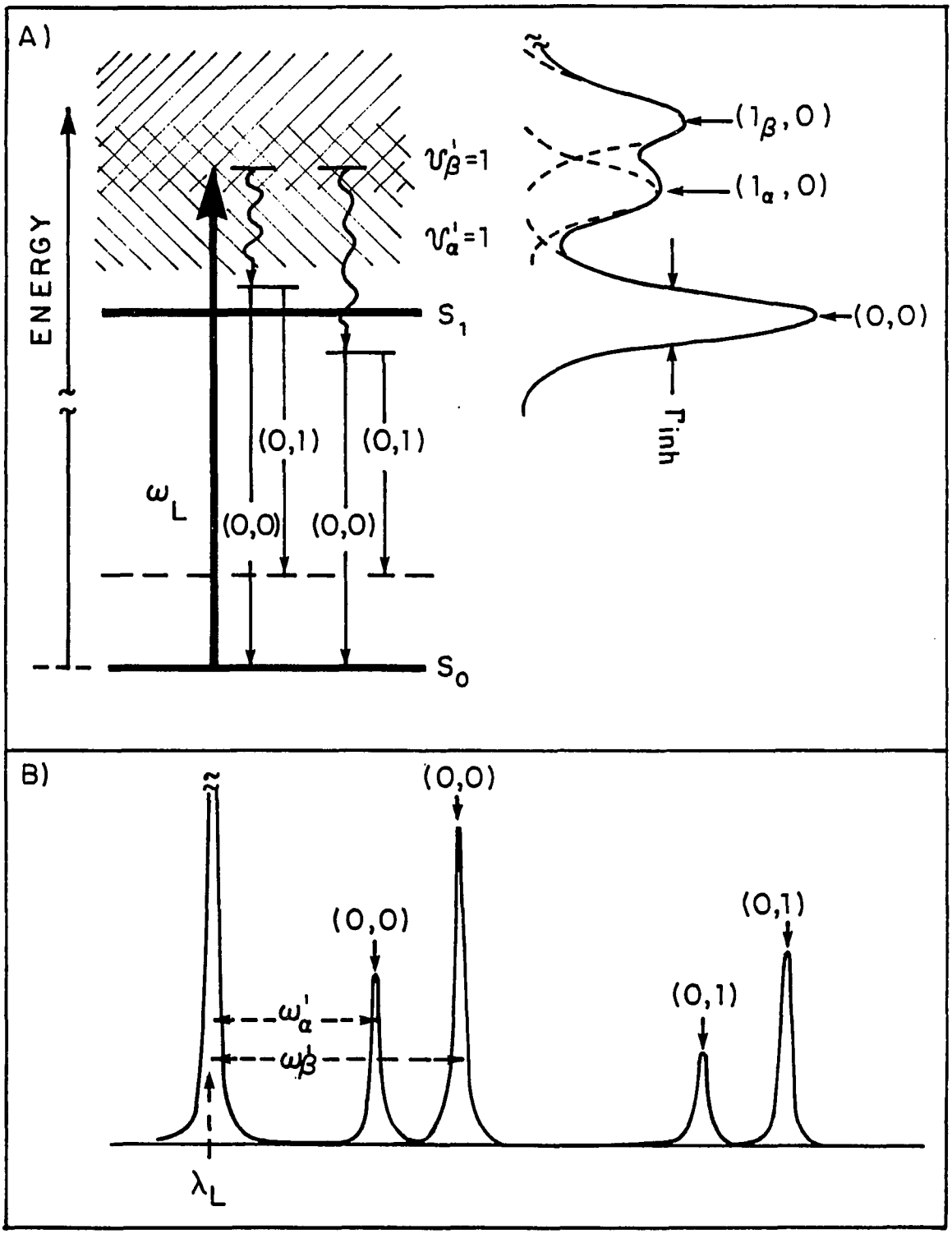
A)
ENERGY
$\nu'_\beta=1$
$\nu'_\alpha=1$
S_1
S_0
ω_L
(0,1)
(0,1)
(0,0)
(0,0)
$(1_\beta,0)$
$(1_\alpha,0)$
(0,0)
Γ_{inh}
B)
(0,0)
(0,0)
(0,1)
(0,1)
ω'_α
ω'_β
λ_L

excited state vibrational frequencies (ω'_α and ω'_β) while the displacements between the (0,0) and (0,1) bands yield ground state vibrational frequencies.

It should be pointed out that the sensitivity of FLN is approximately the same for either origin or vibronic excitation. For the PAH the vibronic Franck-Condon factors in absorption are typically smaller than origin Franck-Condon factors, but this is compensated for by the fact that the fluorescence origin transition is a useful analytical line in spectra generated with vibronic excitation, Figure 5. In addition, by varying ω_L in the vibronic excitation mode it is possible to explore a wide range (~ 400-1300 cm^{-1}) of excited state vibrational frequencies. Thus, a greater degree of characterization and minimization of spectral interference is possible.

II. EXPERIMENTAL

A. Materials and Reagents

The tubes used as sample holders changed as the experimental apparatus and design evolved. Initially polystyrene (Falcon) tubes, 12 x 75 mm, were used. These were followed by quartz melting point tubes (ISU glass shop) open at both ends and mounted horizontally using surface tension to hold the sample in place. The final and best sample container is a 2 mm i.d. quartz tube (ISU glass shop) sealed at one end and held in a vertical position. For some experiments anaerobic sample conditions were needed. To accomplish this samples were exposed to a series of five freeze/pump/thaw cycles prior to completely sealing the tube under anaerobic conditions. Typical sample volumes were .5 ml, 50 μl, and 30 μl, respectively, for each of the sample tubes. The smaller sample volume was desirable to achieve lower detection limits as discussed in the instrumental part of this section. Quartz tubes were necessary for the ultraviolet excitation and emission wavelengths typically encountered with the species investigated. Samples discussed in this dissertation were not degassed unless so indicated.

The solvents used were from different commercial sources. Reagent grade glycerol from Fisher Scientific Company was used without further purification. The 95%

ethanol was obtained from the university storeroom. Water was drawn from the laboratory distilled water supply. Reagent grade dimethylsulfoxide (DMSO) was obtained from Alltech Associates and used without further purification.

Several glass formulations were used depending on the sample being investigated. Most of the samples investigated were diluted into a 45% glycerol, 35% water, and 20% ethanol (by volume) mixture. This mixture forms an optically transparent glass at low temperatures (66). For some experiments a pure water host or a 90% water/10% DMSO mixture was used. The DMSO was found necessary to solubilize some samples. Although neither of these formed an uncracked low temperature glass, they were suitable for viewing relatively long lived fluorescent species (> 10 nsec) when a gated detection system was employed to eliminate laser scatter.

Many samples were used for this research. Sample names, acronyms (to be used throughout the rest of this dissertation), suppliers, and how they were prepared if deemed necesary, are listed according to type: metabolites, DNA adducts, nucleoside adducts, globin adducts, and test compounds used to determine the sensitivity of the instrumentation.

The metabolites consisted of 1,2,3,4-tetrahydro-1,2,3,4-tetrahydroxybenz[a]anthracene (B[a]AT-1); 8,9,10,11-tetrahydro-8,9,10,11-tetrahydrobenz[a]anthracene (B[a]AT-8);

1,2,3,4-tetrahydro-1,2,3,4-tetrahydroxy-5-methylchrysene (5-MeCT); 1,2,3,4-tetrahydro-1,2,3,4-tetrahydroxychrysene (CT); 4,5-dihydro-4,5-dihydroxy-9-methoxybenzo[a]pyrene (B[a]P-diol); 7,8,9,10-tetrahydro-7,8,9,10-tetrahydroxy-benzo[a]pyrene (B[a]PT); 7,8,9,10-tetrahydro-8,9,10-trihydro-7-hydroxybenzo[a]pyrene (7-HTHB[a]P); 7,8,9,10-tetrahydro-7,8,9-trihydro-10-hydroxybenzo[a]P (10-HTHB[a]P); 7,8,9.10-tetrahydro-1,8,9.10-tetrahydrobenzo[a]pyrene (THB[a]P); 6-methylbenzo[a]pyrene (6-MeB[a]P); and benzo[a]pyrene (B[a]P). B[a]AT-1, B[a]AT-8, CT and B[a]PT were obtained from the Midwest Research Institute, Kansas City, Missouri, through the NCI depository. The 5-MeCT was supplied by S. S. Hecht and A. Melikian, Naylor Dana Institute for Disease Prevention. The B[a]P-diol, 7-HTHB[a]P, 10-HTHB[a]P, and THB[a]P were supplied by R. G. Harvey, Ben May Laboratory for Cancer Research, University of Chicago, Chicago, Illinois. The 6-MeB[a]P and B[a]P were obtained from E. Cavalieri and E. Rogan, Eppley Institute for Research in Cancer, University of Nebraska Medical Center, Omaha, Nebraska. All the above listed samples were used without further purification and are shown in Figure 6.

Most of the DNA adducts were made by exposing DNA to the epoxide derivatives of 5-MeCT, CT, B[a]AT-1, B[a]AT-8, and B[a]PT. The structures of these adducts are shown in Figure 7 along with their acronyms derived from the diol epoxide

Figure 6. Acronyms and structures of PAH

Figure 6

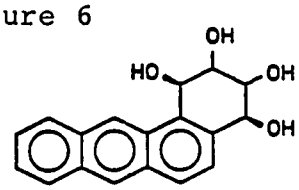

B[a]AT-1

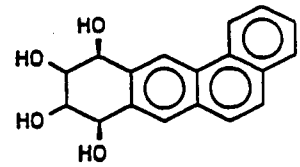

B[a]AT-8

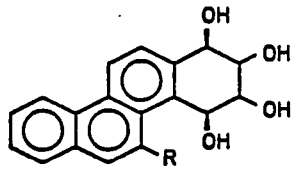

R=CH_3 5-MeCT

R=H CT

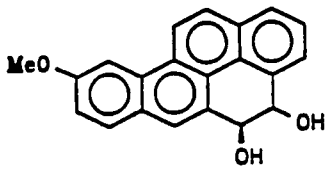

B[a]P-diol

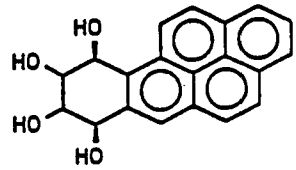

B[a]PT

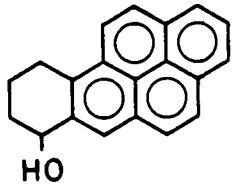

7-HTHB[a]P

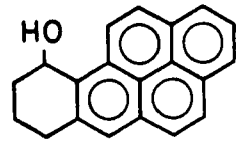

10-HTHB[a]P

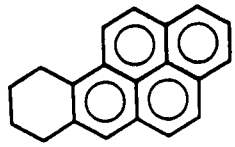

THB[a]P

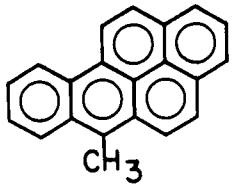

6-MeB[a]P

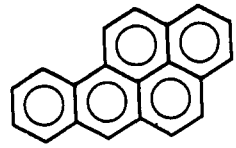

B[a]P

Figure 7. Structures of five DNA adducts. The acronyms for adducts I-V are, respectively, 5-MeCDE-DNA, CDE-DNA, BPDE-DNA, B[a]ADE-8-DNA, and B[a]ADE-1-DNA

Figure 7

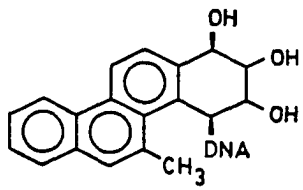

I

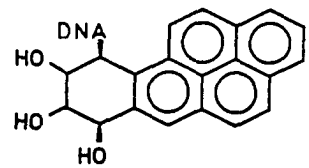

III

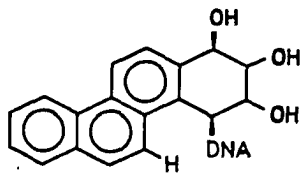

II

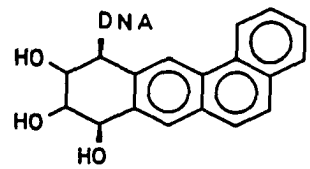

IV

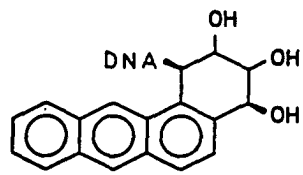

V

DNA Adducts

metabolite involved. Samples of trans-3,4-dihydroxy-anti-1,2-epoxy-1,2,3,4-tetrahydrobenz[a]anthracene (B[a]ADE-1); trans-8,9-dihydrodiol-anti-10,11-epoxy-8,9,10,11-tetrahydrobena[a]anthracene (B[a]ADE-8); trans-1-2,-dihydroxy-anti-3,4-epoxy-1,2,3,4-tetrahydrochrysene (CDE); and trans-7,8-dihydroxy-anti-9,10-epoxy-7,8,9,10-tetrahydrobenzo[a]-pyrene (BPDE) were obtained from the NCI Carcinogen Standard Reference Repository and were used directly. Trans-1,2-dihydroxy-anti-3,4-epoxy-1,2,3,4-tetrahydro-5-methylchrysene (5-MeCDE) was provided by S. S. Hecht. Calf thymus DNA was obtained from Sigma Chemical Company and repurified by phenol extraction and ethanol precipitation prior to use.

DNA (2 mg in 4 mL of 10 mM cacodyate buffer pH 7.0) was modified by the addition of the appropriate diol epoxide (2 mg dissolved in 150 µL of tetrahydrofuran followed by 3.85 mL of acetone). After reaction for 4 hours, the solution was extracted 4 times with ethyl acetate and, after the addition of 200 µL of 2 M sodium at pH 5.4, the DNA was precipitated 3 times with 2 volumes of ethanol. The modified DNA was enzymatically digested to monodeoxy-ribonucleoside derivatives (67) and the modified deoxyribonucleoside derivatives separated by HPLC. The HPLC separations were obtained with an 850 system (Du Pont, Wilmington, Delaware) with an exponential gradient from 30 to 60% methanol in water over 90 min and at 50°C on a Waters

Associates (Milford, Massachusetts) μBondapak C-18 column. Samples were detected by their absorption at 254 nm. The extent of modification of adduct III in Figure 7 was determined by the Randerath procedure (39,40) and was 0.4%.

DNA samples digested after treatment with the 8,9-diol-10,11-epoxide of benz[a]anthracene or the chrysene diol epoxide each gave one major adduct, while that from the 3,4-diol-1,2-epoxide of benz[a]anthracene gave two major adducts in a 3.4:1 ratio. Samples were collected from the HPLC procedure and the solvents removed by evaporation under reduced pressure. The Randerath procedure was not used to determine the modification levels of adducts II, IV, and V in Figure 7 since UV absorption measurements showed that they are comparable to that of adduct III, vide supra.

The low modification level, $5{:}10^6$ and $8{:}10^7$ (adducts:base pairs), DNA adducts of benzo[a]pyrene were obtained from 10T1/2 cell cultures treated with [^{3}H]-benzo-[a]pyrene (1-0.004 mg/mL) for 24 hours. [^{3}H]-benzo[a]pyrene was obtained from Amersham Searle, Arlington Heights, Illinois. Other chemicals were commercially available from standard sources. The cells were grown as previously described in ref. 67 and after treatment with the [^{3}H]-benzo[a]pyrene the cells were washed with PBS and scraped from the plates. The DNA was extracted using methods similar to those described in ref. 67. The nuclei, isolated

by disruption of the cytoplasmic membrane by Triton X-100, were solublized with a 1% SDS solution at pH 6.9, containing 15 mM NaCl and 1.5 mM citrate. This solution was then extracted several times with water-saturated phenol before the DNA was precipitated from the aqueous phase with two volumes of ethanol. The DNA was redissolved and treated with RNase before reextraction with phenol and two ethanol precipitations. The modification levels of these adducts were also determined by the Randerath procedure. All DNA adducts, listed to this point, were made by A. Jeffrey, Institute for Cancer Research, Columbia University, New York, New York.

For studies concerning "one-electron oxidation," the DNA adducts were prepared by exposing DNA to B[a]P in the presence of horseradish peroxidase (HRP) and H_2O_2, followed by a cleanup procedure (32). These samples shall be referred to as HRP-DNA, and were supplied by E. Cavalieri and E. Rogan, Eppley Institute for Cancer Research, University of Nebraska Medical Center, Omaha, Nebraska.

Fish DNA from live fish exposed through controlled environmental conditions to dibenz[a,h]anthracene, benzo[b]-fluoranthene, and benzo[a]pyrene was supplied by U. Varanesi, National Marine Fisheries, Seattle, Washington.

Samples of DNA base adducts of B[a]P (bound at the 6 position) attached at the C-8 positions of guanosine,

deoxyguanosine, and guanine, and at the N-7 position of guanine will be referred to as B[a]P-C-8G, B[a]P-C-8dG, B[a]P-C-8gua, and B[a]P-N-7gua, respectively (see Figure 8). These samples were electrochemically synthesized by selective anodic oxidation of B[a]P in the presence of the nucleoside (32). The pure product was obtained by extraction followed by HPLC or TLC and subsequently by HPLC depending on the adduct desired. These samples were also supplied by E. Cavalieri and E. Rogan.

Globin adduct samples were supplied by R. Santella, Institute for Cancer Research, Columbia University, New York, New York, and were prepared as previously described in ref. 68.

Urine samples used in this research were donated by R. Jankowiak, D. Zamzow, or the author.

Test compounds used to optimize and test the instrumentation were anthracene and 6-methylpyrene. These samples were obtained from Aldrich and API, respectively, and used without further purification.

B. Sample Preparation

Samples were prepared for analysis in the following manner. Samples of metabolites and nucleoside adducts were diluted in the desired glass matrix to a known concentration ($\lesssim 10^{-5}$ M) of the chromophore to be observed. DNA adducts were dissolved in water to a DNA concentration of ~ 1 mg/mL.

Figure 8. Structures and acronyms of nucleoside adducts

Figure 8.

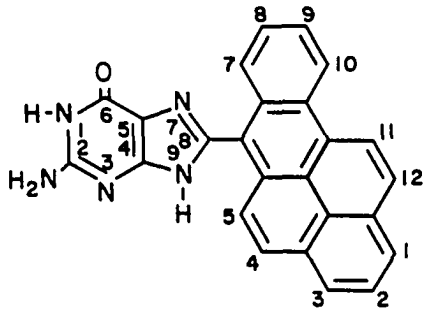

B[a]P-C-8gua

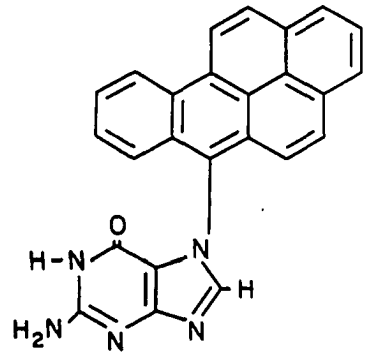

B[a]P-N-7gua

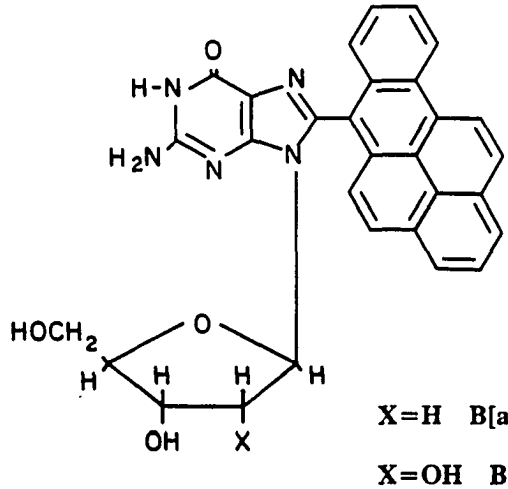

X=H B[a]P-C-8dG

X=OH B[a]P-C-8G

The low modification level DNA adducts were observed in this condition. The higher modification level samples (> $1:10^3$) were diluted with the glycerol/ethanol/water glass formulation to make these samples $\lesssim 10^{-5}$ M in adduct concentration. The sample (~ 30 μL) was placed into a sample tube. Only the 2 mm i.d. quartz tube arrangement will be considered since it is superior to earlier sample containing arrangements. The sample tube is held vertically in an aluminum sample holder designed to occlude scattered laser radiation originating from the sides of the sample tube. This sample holder is attached to the bottom of a long rod and lowered into an optical helium dewar to attain low sample temperatures. Two different dewars were used depending on what sample temperature was desired. If only 4.2 K was needed, a 3 L double nested glass total immersion liquid helium dewar manufactured by Pope Scientific was used. The dewar is constructed so that no liquid nitrogen is in the optical pathway in order to eliminate scattering from nitrogen bubbles. The dewar is equipped with quartz windows so that ultraviolet excitation could be employed. For studies that required sample temperatures other than 4.2 K, a Janis Research model 8-DT Super Vari-Temp liquid helium immersion cryostat equipped with an optical access tail section was utilized. Sample temperatures were measured

using a silicon diode thermometer (Lake Shore Cryogenics model DT-500K) calibrated over the range 1.4 K to 300 K.

C. Instrumentation

To perform fluorescence line narrowing spectrometry some minimum amount of equipment is necessary. The equipment needed can be divided into four major components: a spectrally narrow excitation source, an optically accessible low temperature sample chamber, a dispersion device, and a detection system. The first two components are necessary for the FLN phenomenon to occur, as discussed in the introduction, and the last two components are needed to disperse and detect the emitted fluorescence. Since the sample chamber was discussed in part B of this section only the other three components will be considered. This discussion presents the development of the FLN instrumentation from the initial prototype (69) to its present state shown in Figure 9. The discussion is divided into three parts: excitation, fluorescence collection, and detection. Each part will detail how and why the instrumentation evolved.

Originally two excitation sources were used, a nitrogen laser pumped dye laser system and a Nd-YAG laser pumped dye laser system. The first consisted of a Molectron UV-14 nitrogen laser capable of ~2 mJ/pulse operated at a repetition rate of 30 Hz. This laser emitted radiation at

Figure 9. Block diagram of present FLNS instrumentation showing excimer laser (Exc. L), dye laser (Dye L), cryostat (C), sample (S), photodiode (PD), photodiode array (PDA), monochromator (M), optical multichannel analyzer (OMA), and printer (P). See text for discussion

Figure 9

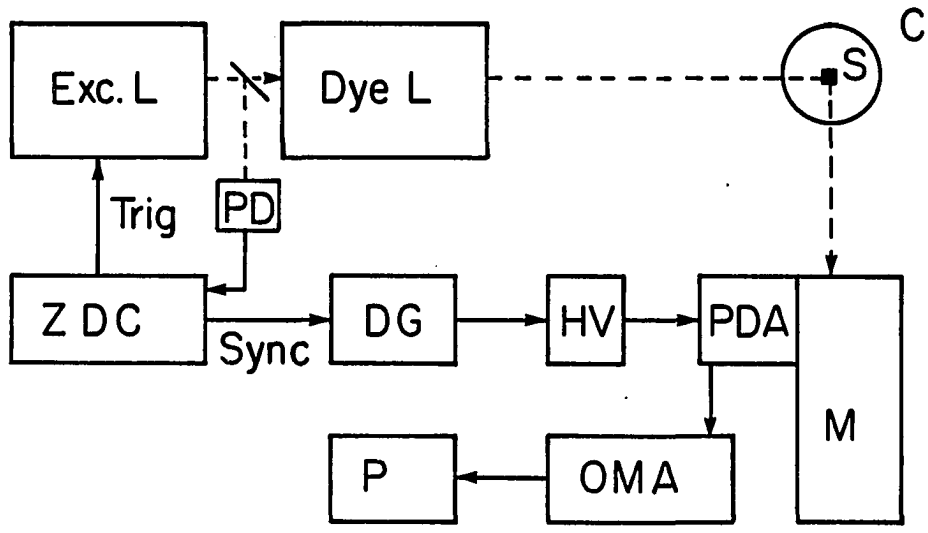

337 nm which was used to pump a molectron DL-200 dye laser. Conversion efficiency of the dye laser was typically ~ 4% and, therefore, average excitation powers were less than 2 mW. Using this dye laser with the Exciton dyes PBD, BBQ, PBBO, Bis-MSD, and DPS a spectral range from 357 to 430 nm was accessible. This was suitable for most of the experiments conducted. For some samples, however, wavelengths less than 357 nm were needed. For these cases the doubled beam of a Quanta Ray DCR Nd-YAG laser with a wavelength of 532 nm was used to pump a Quanta Ray PDL-1 dye laser using LDS-698 (Exciton) as a dye. The output of the dye laser was then doubled using an Inrad model 5-12 frequency doubler. This system allowed the coverage from 322 to 372 nm with average laser powers of 2 mW at 10 Hz. Although both of these excitation systems were adequate for initial experiments, they had some shortcomings. First, it is not desirable to have to use two laser systems. A less complex setup would have one laser to cover all spectral regions of interest. Secondly, neither laser system had sufficient peak powers to fully excite the sample and, therefore, did not yield all the fluorescence possible. As a result, the lowest limit of detection was not obtained. Other problems with the nitrogen laser system arose from the fact that the dye laser emitted a large amount of amplified spontaneous emission and, therefore, only the low energy

sides of dyes were desirable to use. Lastly, the Nd-YAG system could only be operated at 10 Hz. A better arrangement would include high repetition rates to decrease the amount of time needed to acquire a spectrum. To circumvent these problems, a new laser excitation system was obtained.

The new system consists of two basic parts, an excimer laser and a dye laser. The excimer laser is a Lambda Physik EMG 102 MSC excimer laser equipped with an Intelligent Laser Control (ILC). For this research the laser was used with Xe and HCl gases forming the excimer XeCl under a high voltage discharge with He acting as the buffer gas. With these gases, the laser is capable of delivering up to 150 mJ/pulse, when higher pulse energies are needed the buffer gas can be replaced with Ne gas to yield up to 210 mJ/pulse. The output has a temporal width of ~ 10 nsec and can be operated up to 100 Hz. This laser has a synchronous electronic output pulse that is synchronized to the firing of the laser. Unfortunately, the actual laser firing can slowly drift with time and thyratron temperature relative to the electronic synchronous output pulse. For gated detection experiments this was unacceptable and, therefore, a device known as a Zero Drift Control (ZDC) manufactured by Lambda Physik (model EMG 97) was used to compensate for this drift. The ZDC uses a photodiode output pulse and the

electronic synchronous output pulse and introduces them into an electronic comparator which corrects for the long term temporal drift. This ZDC outputs a new "truly" synchronized output pulse. After eliminating this long term drift, the system is left with the shot to shot instability of the thyratron. This instability is about ± 7 nsec, making a 7 nsec delay necessary to completely eliminate laser scatter detection. This 7 nsec delay is much better than the necessary long delays employed previously.

The actual operation of the laser, aside from the timing, is accomplished through the ILC. This device monitors the number of shots fired, thyrotron voltage, output energy, and repetition rate. It will also execute partial and full laser cavity gas refills, when necessary, in order to maintain a constant preset energy level. Probably the most important feature of the ILC is its ability to use comparative feedback from an output energy monitor to maintain a constant energy output.

The beam emerging from the excimer laser is used to pump a Lambda Physik FL 2002 dye laser system. This system is composed of three parts: the dye laser, the scan controller, and a removable etalon. The dye laser is of a Littrow geometry using a grazing incidence grating for wavelength selection. Two dye cells are included in this laser. The first acts as both an oscillator and a

preamplifier. The second acts as an amplifier, all are side pumped. This system yields a 0.22 cm^{-1} spectral linewidth which can be reduced to 0.04 cm^{-1} by inserting the etalon. The dye laser is controlled by a Lambda Physik FL 512A scan controller, which will control both the grating and the etalon. The scan controller is also equipped to accept external control from a computer. Using this dye laser system, wavelengths from 332 to 985 nm are available through the use of several laser dyes and XeCl as the excimer emission source. If KrF is used instead of XeCl and BM-terphenyl (Lambda Physik) is used as the dye laser dye, wavelengths down to 312 nm are accessible.

The output beam of the dye laser is shaped as a symmetrical trapezoid with approximate dimensions of 2 mm by 3 mm. To fully utilize this beam when exciting the sample (cross section 2 mm x 10 mm), it is necessary to form the beam to the shape of the sample. This is accomplished using two quartz 90° turning prisms to direct the beam into the proper pathway, and two lenses, one quartz biconvex and one quartz plano-convex cylindrical lens to form the beam such that its cross sectional dimensions at the sample are as those of the sample to insure complete irradiation.

Following irradiation of the sample, the fluorescence is collected and dispersed. The collection is accomplished with two lenses and the dispersion is produced in a grating

monochromator. The original FLN setup used two 1 inch diameter quartz lenses for collection, one to match the f/5.3 monochromator and the other to collect and collimate. At that time, a narrow laser beam intersecting the sample was used to create a horizontal line of fluorescence in the sample (69). The monochromator was mounted on its side to have a horizontal entrance slit in order to accommodate the horizontal image. A problem arose when the new higher resolution monochromator was obtained since it had vertical slits and can not easily be mounted sideways. To overcome this problem, a dove prism (Melles Griot) was mounted between the two collection lenses in order to rotate the image by 90° as discussed in ref. 70. When the sample tube arrangement was changed to accommodate smaller sample volumes and beam formation was employed a vertical image was formed, therefore the dove prism was no longer necessary.

An important consideration in low level fluorescence detection is capturing as much fluorescence as possible and introducing it into the monochromator. There are two things to keep in mind when approaching this problem. First, one must match the f number of the monochromator. If the monochromator grating is over-filled, light is lost and stray light is introduced inside the monochromator, not a desirable situation from a signal to noise standpoint. On the other hand, if the grating is under-filled, resolution

is lost. Secondly, one must keep in mind that there is a tradeoff between the amount of light collected and the amount that enters the monochromator. This tradeoff is summed up in Figure 10 and Equations 1-5.

Equation 1 is the basic lens equation relating focal

$$\frac{1}{f} = \frac{1}{x} + \frac{1}{y} \tag{1}$$

length (f), object distance (y), and image distance (x). By setting the diameter of the lens (d) equal to x/7, matching of the lens to an f/7 monochromator is insured. Equation 2

$$C = \frac{\pi(d/2)^2}{4\pi y^2} = \frac{d^2}{16y^2} = \frac{(x/7)^2}{16y^2} = \frac{x^2}{784y^2} \tag{2}$$

yields the fraction of total fluorescence collected (C). Equation 3 determines the magnification of the image (m) and

$$m = \frac{x}{y} \tag{3}$$

Equations 4 and 5 calculated the percent of the height (H) and the width (W) of the image that is passed by the slit.

$$H = \frac{a'}{ma} \tag{4}$$

$$W = \frac{b'}{mb} \tag{5}$$

Figure 10. Collection optics diagram. Dimensions are height x width. See explanation in text

Figure 10

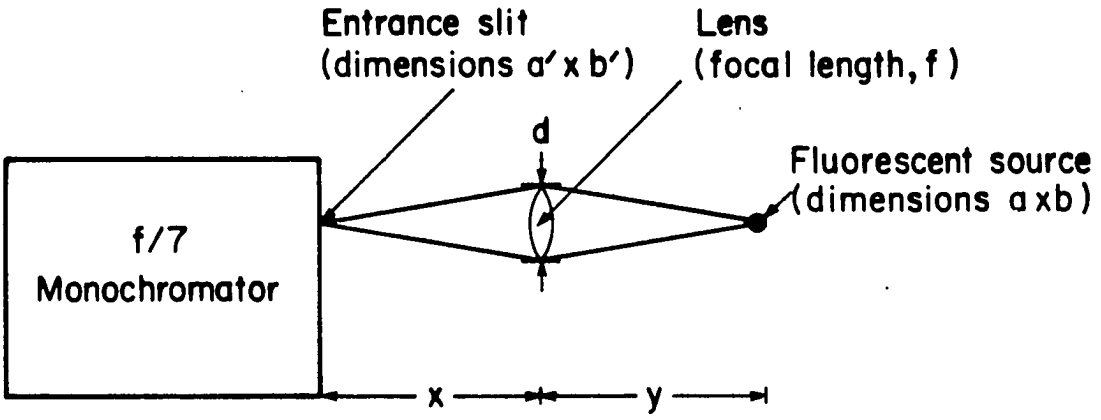
Entrance slit
(dimensions a' x b')
Lens
(focal length, f)
d
Fluorescent source
(dimensions a x b)
f/7
Monochromator
x
y

By multiplying equations 2, 4, and 5 together and using the appropriate boundary conditions, a maximum can be calculated which corresponds to the maximum percentage of light that can be collected and introduced into the monochromator. For the present system a f/3.5 lens placed midway between an f/7 monochromator and fluorescent source separated by 14 times the diameter of the lens would give optimum results. Due to space constraints, two 50 mm diameter lenses, one to collect and collimate and the second to match the monochromator, were used to mimic the one lens system described above. Using the earlier equations an overall collection efficiency of 0.02% was calculated for the system and conditions used. This does not take into account losses at the dewar window and lens interfaces. Also, the actual amount of fluorescence collected was between 1 and 2 times the calculated value since the inside of the aluminum sample holder acts as a back reflector. From the equations presented above, one can see that a reduced sample size without a reduction in the number of fluorescing molecules will allow a greater amount of fluorescence to be passed by the entrance slit. For this reason, smaller sample tubes and higher concentration samples were employed to lower the limit of detection, as mentioned earlier. The collected fluorescence was originally dispersed by a 0.3 meter (f/5.3) McPherson monochromator (model 218). This device had a

linear dispersion of 2.65 nm/mm yielding a resolution of 0.06 nm at entrance and exit slit widths of 10 μ. When it was determined that higher resolutions would be needed for the experiments planned, a 1 meter (f/7) McPherson scanning monochromator (model no. 2061) of the Czerny Turner geometry was obtained. This instrument is equipped with a, 136 mm ruled width x 116 mm groove length, snap-in grating with 2400 grooves/mm and has a transmission range of 185 nm to 650 nm. This system yields a linear dispersion of 0.416 nm/mm and a resolution of 0.005 nm using 7 μ slit widths. The monochromator is scanned by a McPherson (model 788) Digital Drive Control System equipped with an RS 232 computer interface port. One additional feature worth noting is a second detector mount accessed by merely turning a mirror into place, making a switch between two detectors trivial. Before moving on to the detection system, sample alignment should be discussed. Since some of the experiments performed dealt with very low levels of fluorescence, great care had to be taken in the alignment procedure. For optimum alignment a detector was removed and the monochromator is set to zero order. An attenuated HeNe laser beam was directed through the monochromator and collection optics. At the same time, the dye laser (excitation) beam was made to cross the HeNe beam exactly at the focal point of the first collection lens. The sample

inside the dewar was then positioned at the intersection of these beams insuring optimum alignment. The HeNe could then be removed and the detector replaced.

The original detector employed was an Amperex XP-2232 photomultiplier tube (PMT) specially wired for fast response (71). Signals from the PMT were electronically divided by signals from a UDT-UV 20 (Universal Detector Technologies) reference photodiode monitoring the laser beam intensity, in order to cancel out pulse to pulse variations from the laser. The signals were ratioed via a Quanta Ray DGA-1 dual-gated amplifier with a gate time of 100 μsec and an internal delay of 100 nsec or an EG&G Parr model 162 boxcar averager equipped with two model 164 gated integrators and an adjustable internal delay and gate window. Since the synchronous output pulses from all of the lasers used comes before and within 100 μ secs of the light pulses, neither of the signal processors had a problem monitoring the fluorescence. Emission spectra were obtained by scanning the monochromator over the desired wavelength region and using the ratioed output from either device to drive the pen on a Heath chart recorder (model SR-204). Spectra were taken in real time. After the acquisition of the McPherson 1 meter monochromator with two detector ports, a second detection system was added. This second system consists of a Tracor Northern (TN 6134) blue-enhanced

intensified gateable photodiode array (PDA) and a Tracor Northern (TN 6500) optical multichannel analyzer (OMA). The diode array consists of 1024 diodes (25 μ x 2.5 mm) covering ~ 26 mm with an active area of ~ 18 mm. This detector in conjunction with the 1 meter monochromator allows the simultaneous acquisition of ~ 6 nm. Gating is accomplished by the rapid switching of the microchannel plate intensifier. Gate widths from 5 to 120 nsec are available using an Avtech (model AVL-TN-1) high voltage switch. The resolution of the diode array is 4 channels FWHM making the diode array appear to be a 100 μ exit slit. Using a 100 μ entrance slit, the optimum resolution was ~ 0.04 nm. If higher resolution is needed, use of the PMT is necessary. One of the most important features of the PDA system is the gatability. This allows for the discrimination between scattered laser light and low levels of fluorescence and the temporal resolution of species with differing fluorescent lifetimes. Gating is accomplished by using the synchronous output from the ZDC occurring ~ 10 μsec before the laser pulse. This output pulse is fed into a Berkeley Nucleonic Corporation (model 8010) pulse generator (acting as a delay generator) and delayed so that its output triggers an Avtech high voltage switch to turn the detector microchannel plate on nanoseconds after the laser pulse arrives at the sample. Typically the time difference between the laser scatter

arriving at the detector and the detector being activated is 20 nsec. The actual setting of this delay was accomplished by tuning the monochromator to the laser wavelength, setting the detectors temporal gate width to 5 nsec and the detector integration time to some short time period (~ .1 sec), and adjusting the delay until the signal on the OMA screen is maximized. This corresponds to a 0 nsec delay. To accurately set the delay to some delay other than 0 nsec, a tap from the high voltage switch is monitored relative to the synchronous output pulse from the ZDC on a Tektronix (model 2213) oscilloscope, as the delay is changed with the delay generator. Once the desired delay is set the gate width can be opened. The actual acquisition of a spectrum is a two step process. First, a background spectrum is taken (without the sample being irradiated). Then a fluorescence spectrum is taken. The background is subtracted automatically, via the OMA, to account for the varying individual diode responses and to remove any background light admitted to the detector. There are two parameters to adjust when taking a spectrum, integration time per scan and scans per spectrum. Since the signal to noise ratio increases more rapidly as a function of increasing integration time than as a function of the number of scans, the best situation is to use the longest integration time possible with a large number of scans.

Typically, for the experiments performed, the detector begins to saturate at detection times greater than 15 seconds. For this reason, most spectra were obtained with an integration time of 10 sec for 10 scans, making a complete spectrum possible in 200 sec. The PDA is also equipped with a peltier cooler and is cooled to -20°C to reduce dark noise. The OMA itself is a multifunctional data processing system that allows automatic background subtraction, mathematical data processing, histogram data acquisition, magnetic disk data storage and a whole host of other options. A hard copy of data is obtained by output to either a Hewlett-Packard Think Jet printer or a Hewlett-Packard (HP 7470A) dual pen plotter.

For those experiments performed requiring white light restoration pulses, a tungsten-halogen lamp (General Electric) was used as the light source to irradiate the sample via a third window in the sample dewar. In order to prevent this light from reaching the gated detector when it was activated, a Uniblitz high speed shutter (Vincent Associates) was employed. This shutter was activated by the ZDC and delayed such that the shutter was opened 1 msec after the laser light pulse for 1 msec.

III. RESULTS AND DISCUSSION

A. Introduction

FLN spectrometry has demonstrated the ability to identify amino PAH (72) and to analyze for nonpolar PAH in both laboratory mixtures and a solvent-refined coal sample (63,73). More recently, it was shown that FLN spectrometry was applicable to active metabolites of B[a]P and the adducts they form with DNA (61). In addition, a mixture of two B[a]P metabolites was analyzed using FLN. These results demonstrated that FLN spectrometry in glasses has exciting potential for the direct high-resolution analysis of nucleic acid damage resulting from chemical carcinogens.

Several important questions, however, were left unanswered by this prior research. One relates to the generality of FLN spectrometry. That is, can FLN spectrometry generally be applied to the polar metabolites of PAHs and the DNA adducts and other biologically important adducts? Furthermore, does FLN spectrometry possess the selectivity to identify the PAH metabolite and adduct components of reasonably complex mixtures? This will be important if the synergistic and antagonistic effects on DNA damage are to be studied in the future. Finally, does FLN spectrometry possess the sensitivity to detect DNA damage at the low levels required for practical applications to real samples? The intent of this dissertation is to explore

these questions. To this end, the results of FLN studies on a six metabolite mixture, a five component intact DNA adduct mixture, and finally an eight component mixture of both metabolites and DNA adducts are presented and discussed to establish the selectivity of FLN for these types of species (70,74). Following this is a discussion of the measures required to achieve a femtomole limit of detection for the BPDE-DNA adduct and the steps that had to be taken in order to retain the high selectivity of the FLN method when using the high laser excitation power densities needed to obtain this limit of detection (75). Lastly, the application of FLN to the investigation of BPDE-globin adducts, metabolites in urine, real samples, and metabolic pathways is presented to demonstrate the broad applicability of FLN spectrometry (75).

B. Selectivity

As a first test of the selectivity of the FLN method, the resolution of a mixture of six polar PAH metabolites, B[a]AT-1, B[a]AT-8, 5-MeCT, CT, B[a]P diol, and B[a]PT (shown in Figure 6), was attempted (70). The underlying physics of the FLN phenomenon were described in the introduction. There it was shown that excitation into the origin (0,0) band of the fluorescent state with a narrow-line laser selects out a comparably narrow isochromat, and the fluorescence spectrum is narrowed. It was also shown

that excitation into low-lying vibronic bands, (1,0) excitation, also yields FLN. For many molecules, a low-lying (1,0) absorption band several hundred inverse centimeters above the (0,0) band which is due to a single vibration can be found. Excitation of such a (1,0) band affords a FLN spectrum which matches in simplicity the spectrum obtained with (0,0) excitation. However, for (1,0) excitation, the origin or (0,0) fluorescence band is displaced to lower energy of the laser frequency by an amount equal to the frequency of the excited vibration. This is important because the (0,0) fluorescence band is now a useful analytical line. For (0,0) excitation, the fluorescence origin is typically contaminated by laser light scatter. The complexity which arises when the vibronic absorption feature being pumped is comprised of several overlapping and unresolvable (1,0) bands has been considered (63). Laser excitation of such a vibrationally congested feature pumps as many different isochromats as there are overlapping bands. In the extreme, where the number of bands is very large, line narrowing is lost and the fluorescence spectrum has the broad and disappointing appearance of the spectrum obtained with a broad-band excitation source which uniformly excites all sites. Importantly, however, when the number of bands is small (~

3), the analytical utility of FLN spectrometry is enhanced when (1,0) rather than (0,0) excitation is utilized.

Fluorescence excitation spectra, not given here, were used as a guide for the determination of several suitable excitation wavelengths (λ_{ex}) for each of the six PAH metabolites. Earlier work (66) emphasized the importance for analyses of generating standard FLN spectra for at least two excitation wavelengths, and this will be underscored again in what follows. The fluorescent parent chromophores associated with the metabolites are either anthracene, chrysene, pyrene, or phenanthrene. It was important for assessing sample purity to first obtain FLN spectra with (0,0) excitation so that the vibrational frequencies and relative intensities could be compared with those of the parent chromophores. Fluorescence line narrowing was exhibited by all metabolites studied. Typical of the spectra obtained are those shown in Figure 11 for B[a]AT-1 and CT, while a partial vibrational analysis for each of the metabolites is given in Table 2. On the basis of the close agreement between the metabolite FLN spectra and those of their respective parent chromophores, the sample purities are judged to be high. We note that B[a]AT-8, CT, and 5-MeCT possess the phenanthrene chromophore and, therefore, that their spectra are quite similar. However, these three

Figure 11. Standard FLN spectra of B[a]AT-1 (top) and CT (bottom) following (0,0) excitation at 4.2 K. L labels laser peak. Vibrational lines are labeled in energy units of inverse centimeters relative to the excitation energy. See Table 2 for partial vibrational analysis of all six metabolites

Figure 11

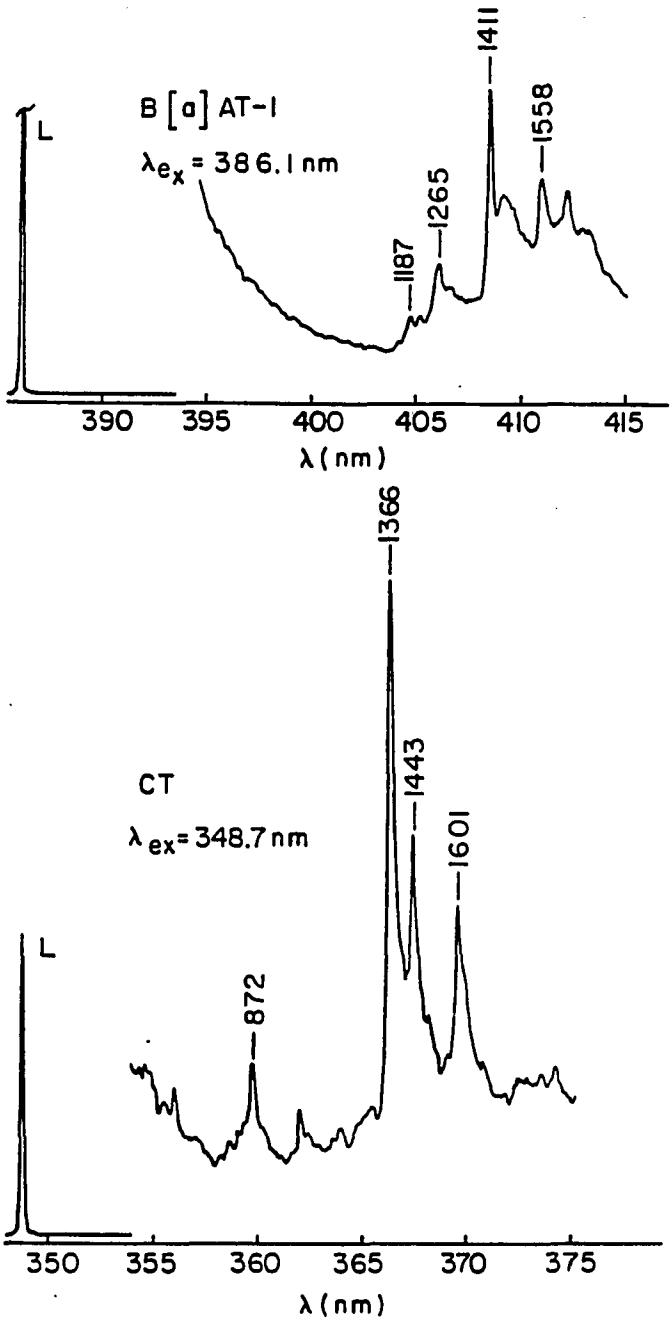
B [a] AT-I
λex = 386.1 nm
L
1411
1558
1265
1187
390
395
400
405
410
415
λ (nm)
CT
λex = 348.7 nm
L
1366
1443
1601
872
350
355
360
365
370
375
λ (nm)

Table 2. Partial vibronic analysis of components following (0,0) excitation

compound $\lambda_{ex}(0,0)$, nm	concentration (μm) pure	concentration (μm) mixture	vibration frequencies, cm^{-1}
B[a]AT-1, 386.1	103	9	1187 (w), 1265 (m), 1411 (s), 1558 (m)
B[a]AT-8, 351.7	109	41	1358 (s), 1441 (m), 1607 (m)
5-MeCT, 356.9	170	26	648 (w), 887 (w), 1364 (s), 1440 (m), 1594 (m)
CT, 348.7	104	16	872 (w), 1366 (s), 1443 (m), 1601 (m)
B[a]P-diol, 373.5	308	4	329 (m), 492 (w), 536 (w), 878 (w), 1391 (s)
B[a]PT, 377.1	220	46	597 (w), 792 (m), 856 (m), 1116 (m), 1249 (s), 1291 (m), 1414 (s), 1563 (m)

Assignments are ± 10 cm^{-1}. Intensities are designated (w), < 0.2 of major peak; (m), 0.2-0.5; (s), > 0.5 of major peak.

metabolites can be distinguished on the basis of selective excitation of their (0,0) absorption bands.

In all tables and figures, and throughout the text laser excitation wavelengths will be given in nanometers. However, the lines in the FLN spectra are due to vibrations of the molecule and are thus labeled in units of vibrational energy, wavenumbers (cm^{-1}). This vibrational energy is the difference in energy between the excitation and emission wavelengths. For (0,0) excitation, as in Table 2 and Figure 11, the energies, therefore, may be directly interpreted as ground-state vibrational frequencies.

For any low-temperature high-selectivity fluorescence technique, the electron-phonon interaction is a potential problem for selectivity (76,77). If sufficiently strong, it produces broad low-frequency phonon sidebands (PSBs) which build on the sharp zero-phonon vibronic features of the fluorescence spectrum. For very strong coupling, the zero-phonon lines (ZPLs) are lost, as is the high selectivity of FLN. The metabolite which exhibits the strongest coupling, moderately strong, is B[a]AT-1, which possesses the anthracene chromophore. This observation is consistent with earlier results on anthracene and substituted anthracenes (73). The moderate electron-phonon coupling for B[a]AT-1, Figure 11, posed no problem for the analysis of the six-component metabolite mixture. The benzo[a]pyrene

metabolites were previously shown to exhibit weak coupling (61).

For a fluorescence-based technique, the distinction between the unsubstituted chrysene metabolite, CT, and its analogue, 5-MeCT, is a formidable challenge and important since 5-methylchrysene is a potent carcinogen while chrysene is not (78,79). However, the (0,0) absorption band of 5-MeCT is significantly red-shifted (~ 600 cm^{-1}) relative to CT so that in a binary mixture of the two metabolites, 5-MeCT can be determined without any interference from CT when origin excitation for 5-MeCT is used. The key question is whether a λ_{ex} suitable for FLN from CT will allow for its characterization since this excitation will excite 5-MeCT with considerable excess vibrational energy. The concentrations of the two components are low enough to preclude any effects of interaction on the spectra. But because 5-MeCT is excited with excess vibrational energy, the utility of FLN for analysis may be negated if the fluorescence of 5-MeCT is broad enough to obscure narrow lines arising from CT. This will be an ever-present problem in doing direct mixture analysis, and different mixtures may have to be characterized at different excitation wavelengths.

Figure 12 shows the FLN spectrum of the binary mixture for a λ_{ex} coincident with the (0,0) absorption band of CT.

Figure 12. FLN spectrum of mixture of CT (60 μm) and 5-MeCT (73 μm), following excitation of the (0,0) transition of CT

Figure 12

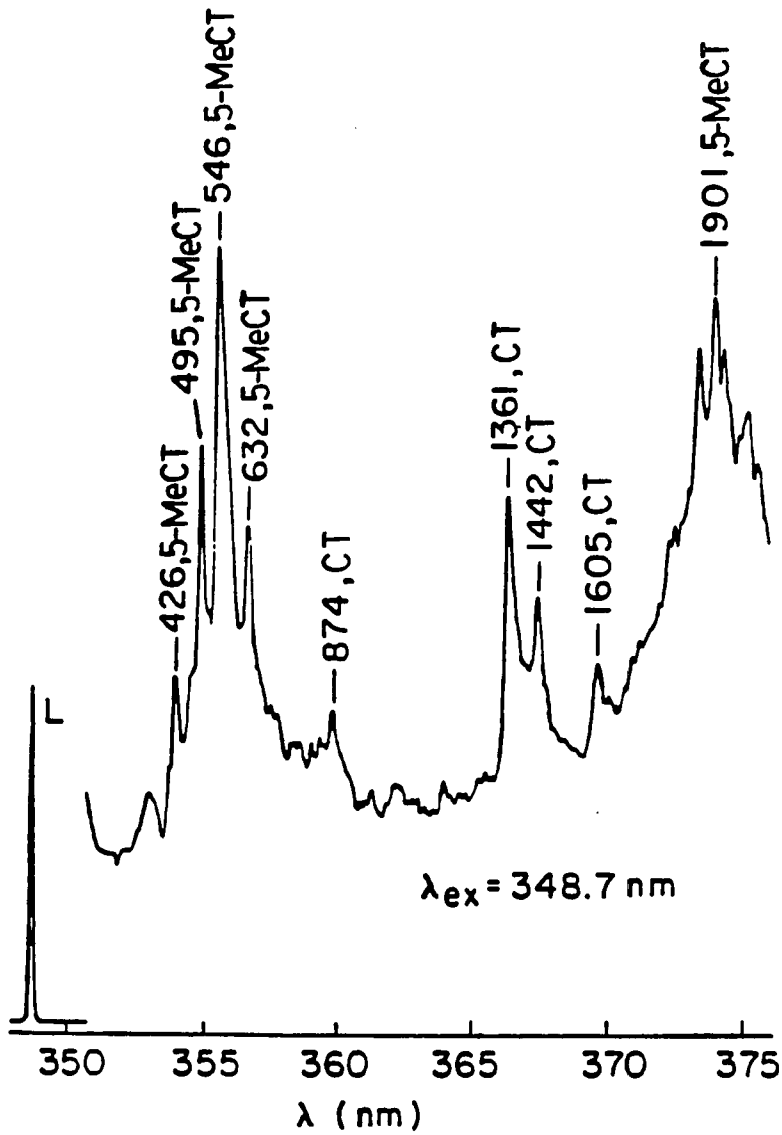
426,5-MeCT
495,5-MeCT
546,5-MeCT
632,5-MeCT
874,CT
1361,CT
1442,CT
1605,CT
1901,5-MeCT
λex = 348.7 nm
350
355
360
365
370
375
λ (nm)

All four main peaks for the CT spectrum are evident, as shown in Table 2. Interestingly, the set of four line-narrowed bands near 355.5 nm comprises the (0,0) fluorescence multiplet structure for 5-MeCT arising from the excitation of a vibrationally congested vibronic absorption band, as described previously. The energy differences between these bands and the laser excitation frequency provide the frequencies of the overlapped excited state vibrations which are 426, 495, 546, and 632 cm^{-1}. The multiplet structure provides a fingerprint for identification which may be more useful than the pattern arising from (0,0) excitation. The broad fluorescence at ~ 373.5 nm in Figure 12 results from the overlap of fluorescence lines from each of the four excited-state vibrational isochromats excited by the laser. Note that the peak at 1901 cm^{-1} in the spectrum of Figure 12 is separated from the highest intensity 5-MeCT (0,0) fluorescence multiplet component at 546 cm^{-1} by ~ 1356 cm^{-1}, which is the major ground-state fluorescence line, shown in Table 2.

We turn now to the analysis of a six-component PAH metabolite mixture, as given in Table 2. In view of earlier work on FLN of DNA-PAH metabolite adducts (61), resolution of the six metabolites would augur well for the resolution of a comparable mixture of adducts. Previous applications of FLN have emphasized the use of a λ_{ex} which excites a

single isochromat (66,73). Indeed, for a binary mixture of B[a]PT and B[a]P-diol, excitation of the two (0,0) absorption bands resulted in each case in a single-component FLN spectrum, with no interference from the second component (61). However, mixtures generally do not lend themselves to such convenient analysis. Interference from broad fluorescence from other components can obscure the FLN spectrum of the component of interest. For example, if in the analysis of 5-MeCT, λ_{ex} = 356.9 nm is used, providing (0,0) excitation for 5-MeCT, then serious interference from the fluorescence of B[a]P-diol occurs. This λ_{ex} excites B[a]P-diol in a vibrationally congested region with ~ 1300 cm^{-1} of excess vibrational energy, cf. Table 2. Because of interferences of this nature, (1,0) excitation for the components of interest proved to be the key to resolving the mixture. In this regard, the multiplet origin structure afforded by (1,0) excitation was particularly helpful.

In the process of analysis of the mixture, about 30 fluorescence spectra were obtained, and, except for B[a]AT-8, every component was identified by its FLN spectra at two or more excitation wavelengths. As examples, Figures 13 and 14 are presented in order to discuss the analysis procedure. The FLN spectrum in Figure 13 for the mixture was obtained with λ_{ex} = 342.2 nm which provides (1,0) excitation for CT with ~ 550 cm^{-1} of excess vibrational

Figure 13. FLN spectrum of mixture of six PAH metabolites. Peaks are labeled as being due to B[a]AT-8, 5-MeCT, or CT. Inset: partial spectrum of pure CT, showing lines used for identification

Figure 13

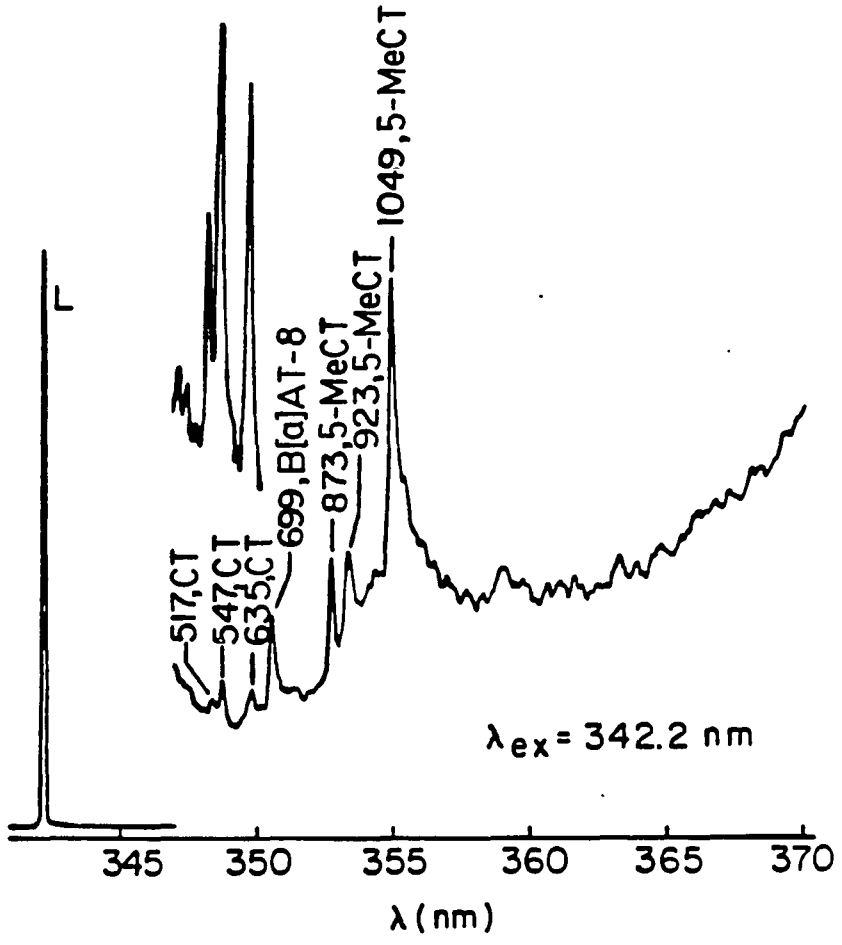
517,CT
547,CT
635,CT
699,B[a]AT-8
873,5-MeCT
923,5-MeCT
1049,5-MeCT
λex = 342.2 nm
345
350
355
360
365
370
λ (nm)

Figure 14. FLN spectrum of six-component mixture. Peaks are labeled as B[a]AT-1, B[a]P-diol, and B[a]PT. Inset: partial spectrum of B[a]P-diol, showing lines used for identification

Figure 14

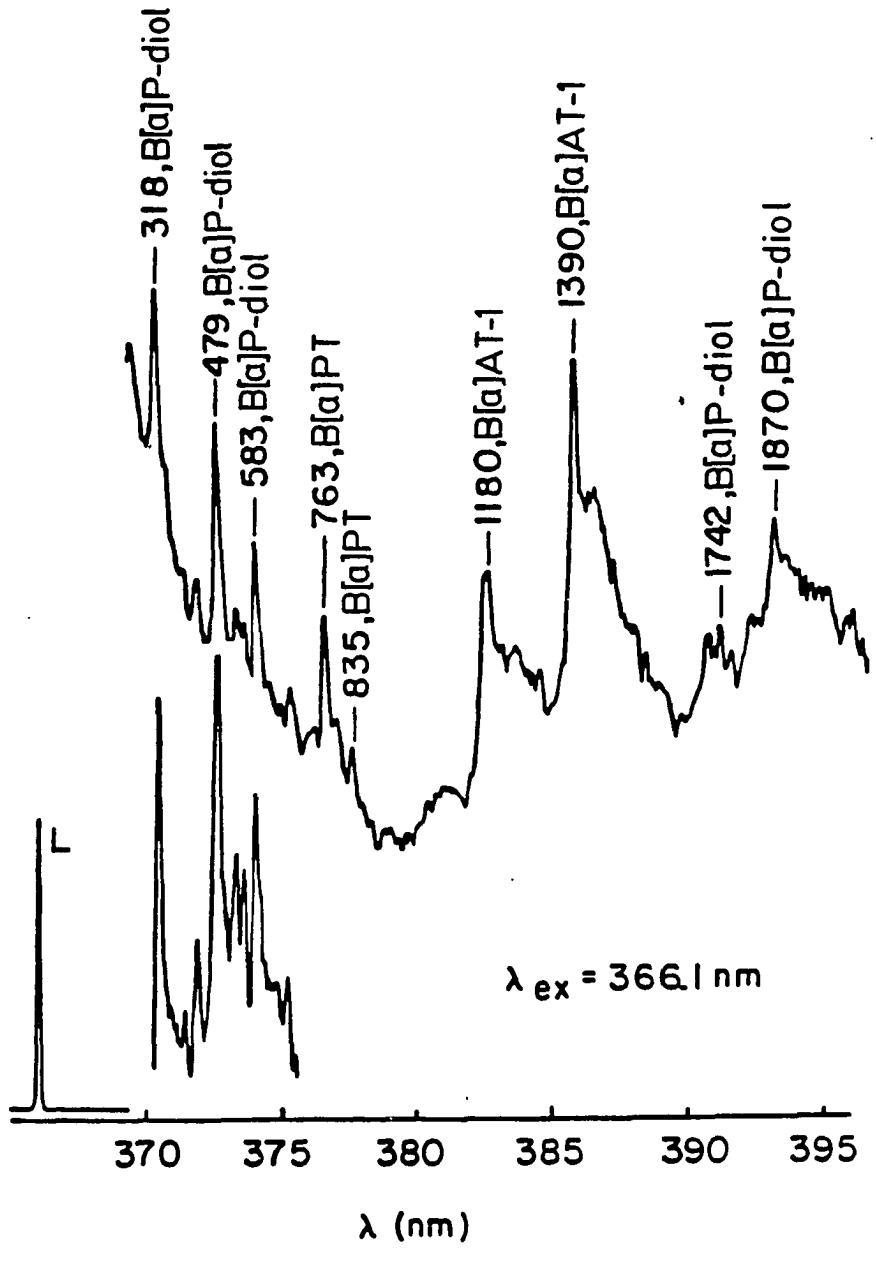
318,B[a]P-diol
479,B[a]P-diol
583,B[a]P-diol
763,B[a]PT
835,B[a]PT
1180,B[a]AT-1
1390,B[a]AT-1
1742,B[a]P-diol
1870,B[a]P-diol
λ ex = 366.1 nm
370
375
380
385
390
395
λ (nm)

energy. The inset spectrum was obtained for CT by itself and with the same excitation wavelength. Thus, the 517-, 547-, and 635-cm^{-1} bands represent the origin multiplet structure for CT, and these frequencies correspond to the excited-state vibrations being pumped. For completeness, the FLN spectra for λ_{ex} = 342.2 nm were obtained for pure B[a]AT-8 and 5-MeCT and were used to assign the remaining bands in Figure 13. This would not be necessary if one is interested in analyzing only for CT. In Figure 14, the λ_{ex} = 366.1 nm was chosen to provide (1,0) excitation for B[a]P-diol, and the inset spectrum obtained for the pure diol establishes its assignments in the mixture spectrum. The multiplet origin structure for B[a]P-diol is particularly rich. The assignments in the mixture spectrum for B[a]PT and B[a]AT-1 were made on the basis of the λ_{ex} = 366.1 nm FLN spectra of the pure compounds. The procedure just described was followed for the analysis of the mixture for each of the metabolites.

Following the successful resolution of six metabolites, a five component mixture of DNA adducts was attempted (74). The five DNA adducts used in this study are shown in Figure 7. The parent chromophores are phenanthrene, anthracene, and pyrene. As in the study of mixtures of PAH metabolites, the DNA adducts were individually characterized, and several excitation wavelengths were selected for each. As expected,

fluorescence line narrowing was exhibited by each of the adducts. However, for adduct V, there is a significant intensity in the PSBs, and the ZPLs, although sharp, are weak. As discussed earlier the ratio of ZPL intensity to that of PSB of the corresponding metabolite was also fairly low, and therefore the intense PSBs were not unexpected. Although this did not prove to be an obstacle in analyzing mixtures of DNA adducts, it did make identification of the adduct in the presence of the tetrol more difficult. None of the other adducts or tetrols studied exhibited significant PSB intensity.

It is interesting to note that although there is good correlation between the vibrational frequency spacings for the DNA adducts and those of the unbound tetrol, there is also a small but consistent red shift (about 100-300 cm^{-1} depending on the adduct) in the $S_1 \leftarrow S_0$ absorption spectrum of the adduct. The red shifts observed for all the DNA adducts were important in allowing adducts to be spectroscopically distinguished from their corresponding tetrols.

Standard FLN spectra have been generated for the DNA adducts shown in Figure 7. For each adduct spectra were obtained for at least two excitation wavelengths and a partial vibrational analyses completed as shown in Table 3. The resolution of a mixture of these five adducts is not a

Table 3. Partial vibronic analysis of components

DNA adduct (0,0), nm	Concentration in mixture (μM)	Vibration frequencies, cm^{-1}
B[a]ADE-1-DNA, 391	17	ES: 1390, 1180, 596, 485, 439 GS: 1558, 1420, 1270
B[a]ADE-8-DNA, 352	34	ES: 1600, 1520, 1438, 1386, 1281, 1160, 1022, 866, 694, 618 GS: 1603, 1444, 1359, 1248, 1044, 880, 729, 638
CDE-DNA, 350	7	ES: 1384, 943, 846, 703, 633, 546, 519 GS: 1605, 1442, 1365, 1044, 873, 582, 233
5-MeCDE-DNA, 356	16	ES: 1392, 1354, 1043, 922, 871, 800, 631, 562, 490, 447 GS: 1604, 1448, 1372, 1364, 1069, 889, 655
B[a]PDE-DNA, 378.5	3	ES: 1109, 1045, 957, 830, 761, 579, 465 GS: 1637, 1560, 1413, 1249, 1120, 855, 787, 596

ES and GS represent excited state and ground state vibrations, respectively.

trivial problem since the B[a]ADE-DNA (I), CDE-DNA (II), and B[a]ADE-8-DNA (IV) adducts each possess phenanthrene as the parent fluorescent chromophore. Nevertheless, Figure 15 demonstrates that with an excitation wavelength of 343.1 nm these three adducts are readily distinguished. This figure contains portions of the standard FLN spectra for each of the adducts that are readily correlated with the peaks which appear in the mixture spectrum. The above excitation wavelength provides (1,0) type excitation for each adduct, and the FLN structure (peaks labeled with excited-state vibrational frequencies in cm^{-1}) corresponds to multiplet origin structure. In part the resolution of adducts I, II, and IV depends on their $S_1 \leftarrow S_0$ absorption spectra being shifted relative to each other. It is adduct I whose absorption lies furthest to the red, consistent with its labeled vibrational frequencies being the highest (1040 and 1348 cm^{-1}). Figure 16 shows a portion of the FLN mixture spectrum obtained for an excitation wavelength of 369.5 nm. With this spectrum B[a]PDE-DNA (III) and B[a]ADE-1-DNA (V) are readily distinguished. Again (1,0) type excitation for both adducts is provided by λ_{ex} = 369.5 nm. Sharp zero-phonon lines for B[a]ADE-1-DNA at 1181 and 1391 cm^{-1} are apparent, superimposed on the broad phonon side profile, centered near 395 nm. It is possible that different host glasses may lead to a diminution of phonon sideband activity

Figure 15. FLN spectrum from a mixture of the five DNA adducts obtained with (1,0) type excitation at 343.1 nm, T = 4.2 K. Peaks labeled A, B, and C are due to the three individual adducts pictured. See text and Table 3 for further details

Figure 15

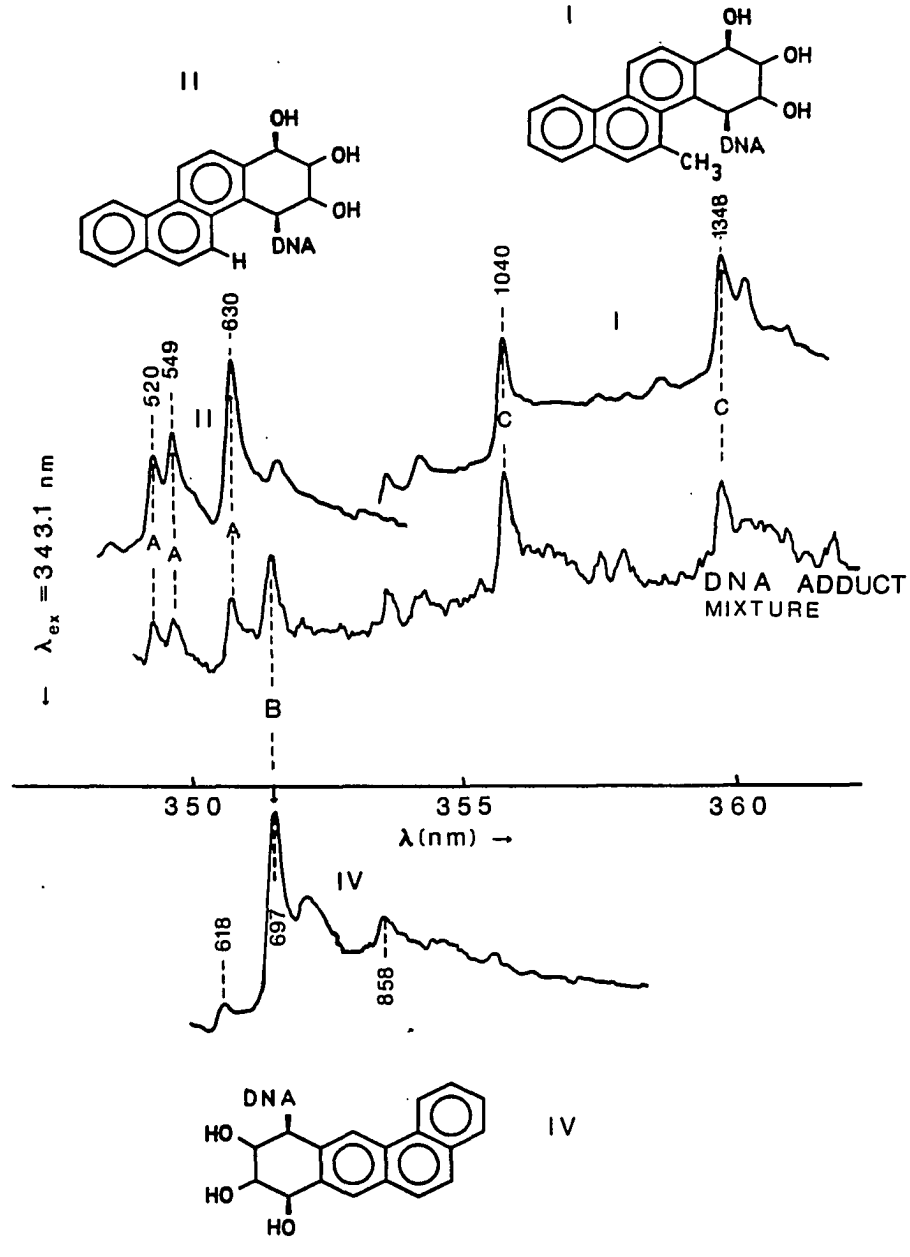
I
OH
OH
OH
DNA
CH3
II
OH
OH
OH
DNA
H
1348
1040
630
520
549
I
II
C
C
A
A
A
DNA ADDUCT
MIXTURE
λex =343.1 nm
B
350
355
360
λ(nm) →
IV
618
697
858
DNA
HO
HO
HO
IV

Figure 16. FLN spectrum from a mixture of the five DNA adducts obtained with (1,0) type excitation, T = 4.2 K. Peaks are labeled as being due to either B[a]PDE-DNA (III) or B[a]DE-1-DNA (V) as indicated by the inset spectra for pure adducts III and V

Figure 16

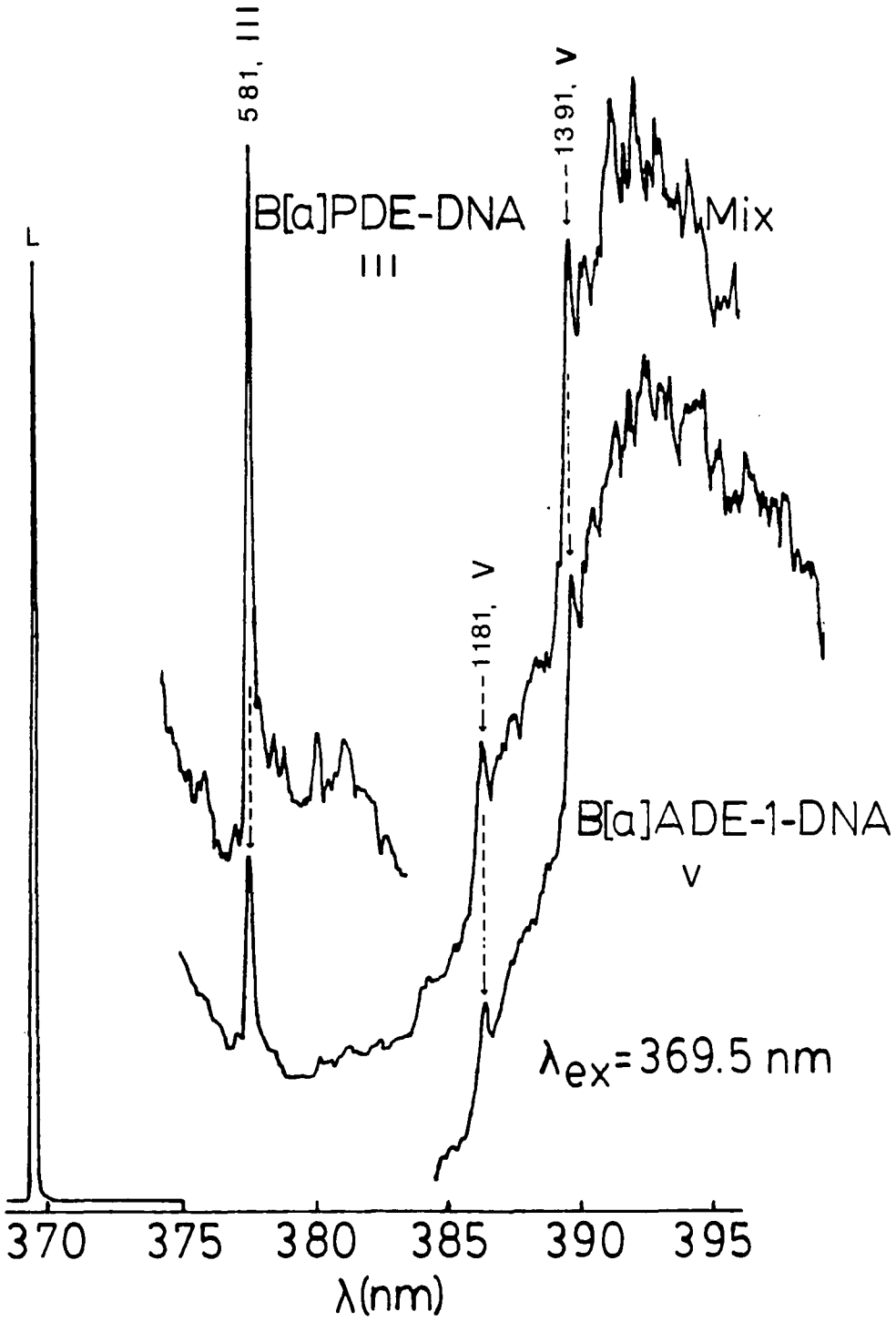
581, III
1391, V
B[a]PDE-DNA
III
Mix
L
1181, V
B[a]ADE-1-DNA
V
λex=369.5 nm
370
375
380
385
390
395
λ(nm)

for adduct V. Note that this activity for B[a]PDE-DNA is weak with the FLN spectrum dominated by zero-phonon lines (e.g., at 581 cm^{-1}, which is an excited-state vibration).

Thus, as was the case for the mixture of the tetrols associated with the adducts of Figure 15, it shown that (1,0) type vibronic excitation affords facile resolution for a comparably complex adduct mixture.

A further test of the selectivity of FLN spectrometry was the identification of DNA adducts in the presence of the corresponding tetrols. For each of the five pairs of compounds tested, the DNA adduct could be identified in mixtures containing approximately equal amounts of each. The basis for this identification is the small red shift in the absorption spectra and differences in the excited state vibrations of the DNA adducts as compared with the tetrols, as demonstrated in Table 4 for BPDE-DNA and B[a]PT. Excitation into a region of origin or (0,0) absorption for both the bound and unbound metabolites yields a fluorescence spectrum with lines from both generally overlapped. The ground-state vibrational energy differences between the bound and unbound metabolite determine the displacements between overlapped lines. Typical displacements are small, $\lesssim$ cm^{-1}.

The reason is that (0,0) or origin excited fluorescence spectra from a given parent PAH are not significantly

Table 4. Ground and excited state vibrational frequencies (cm^{-1}) of B[a]P tetrol and BPDE-DNA in glass at T = 4.2 K

B[a]P Tetrol				BPDE-DNA			
Ground State Vibrations (cm^{-1}) λ_{ex} = 377.1 nm		Excited State Vibrations (cm^{-1})		Ground State Vibrations (cm^{-1}) λ_{ex} = 377.1 nm		Excited State Vibrations (cm^{-1})	
464	s	454 m	(1)	468	w	452 m	(7)
477	s	471 m	(1)	478	w	465 s	(7)
510	m	---	(1)	512	w	476 m	(7)
559	s	---	(1)	562	s	504 m	(7)
594	s	532 m	(1)	596	s	---	(7)
745	m	546 m	(1)	751	m	541 m	(7)
786	s	578 s	(1)	787	m	579 s	(7)
848	s	757 s	(2)	855	s	761 s	(8)
1118	s	827 m	(2)	1118	s	830 s	(8)
1179	m	956 s	(3)	1179	m	957 s	(8)
1249	s	1049 m	(3)	1249	s	1045 s	(8)
1290	m	1111 s	(3),(4)	1289	m	1109 s	(8)
1414	s	1158 s	(4)	1413	s	---	(9)
1556	s	1179 m	(4)	1560	s	---	(9)
1592	m	1330 m	(5)	1592	m	---	(9)
1631	m	1379 m	(5)	1637	m	1379 s	(9)
		1441 m	(5),(6)			1435 s	(9)
		1517 m	(6)			---	(10)
		1562 s	(6)			---	(10)
		1615 s	(6)			1617 m	(10)

Excited state vibrational intensities are dependent on λ_{ex}.

s = strong
m = medium
w = weak

(1): λ_{ex} = 368.3 nm
(2): λ_{ex} = 365.6 nm
(3): λ_{ex} = 362.5 nm
(4): λ_{ex} = 360 nm
(5): λ_{ex} = 358 nm
(6): λ_{ex} = 355.4 nm
(7): λ_{ex} = 371.5 nm
(8): λ_{ex} = 365.5 nm
(9): λ_{ex} = 359.5 nm
(10): λ_{ex} = 353.5 nm

perturbed by substituent groups. That is, the ground state vibrational frequencies and (0,1) vibronic intensities are not very sensitive to ring substitutions. On the other hand, the vibrational structure and dynamics in the S_1 state are often sensitive to ring substitution. The reason appears to be connected with Herzberg-Teller vibronic coupling, vibronically induced anharmonicity and the symmetry reduction resulting from substitution (80). Thus the S_1 states of PAH such as naphthalene, phenanthrene, pyrene and benzo[a]pyrene, whose $S_1 - S_2$ energy gaps are only a few thousand cm^{-1}, are expected to exhibit the above sensitivity. Vibronic coupling effects become more pronounced as the energy gap between the two coupled electronic states decreases. For the DNA-PAH adducts and unbound metabolites, vibronic excitation at ~ 500 cm^{-1} above the (0,0) transition revealed a rich and very diagnostic multiplet origin structure in fluorescence consisting of several bands (analogous to the doublet shown in Fig. 2B).

With these facts in mind it becomes apparent that by using (1,0) excitation the excited-state vibrations that are pumped, by a specific λ_{ex}, in a DNA adduct will be different from those in the corresponding tetrol. Therefore, the distinction between the two is trivial based on origin multiplet structure. An example of this is shown in Figure 17 for 5-MeCDE-DNA and 5-MeCT using λ_{ex} = 342.2 nm. The

Figure 17. FLN spectra of a mixture of a DNA adduct and corresponding tetrol. Top spectrum (pure 5-MeCT) and bottom spectrum (pure 5-MeCDE-DNA) shows lines labeled in cm^{-1} used for identification. See text for further discussion. Results, not given, have been obtained which establish that each and every adduct of Figure 7 can be distinguished from its corresponding tetrol

Figure 17

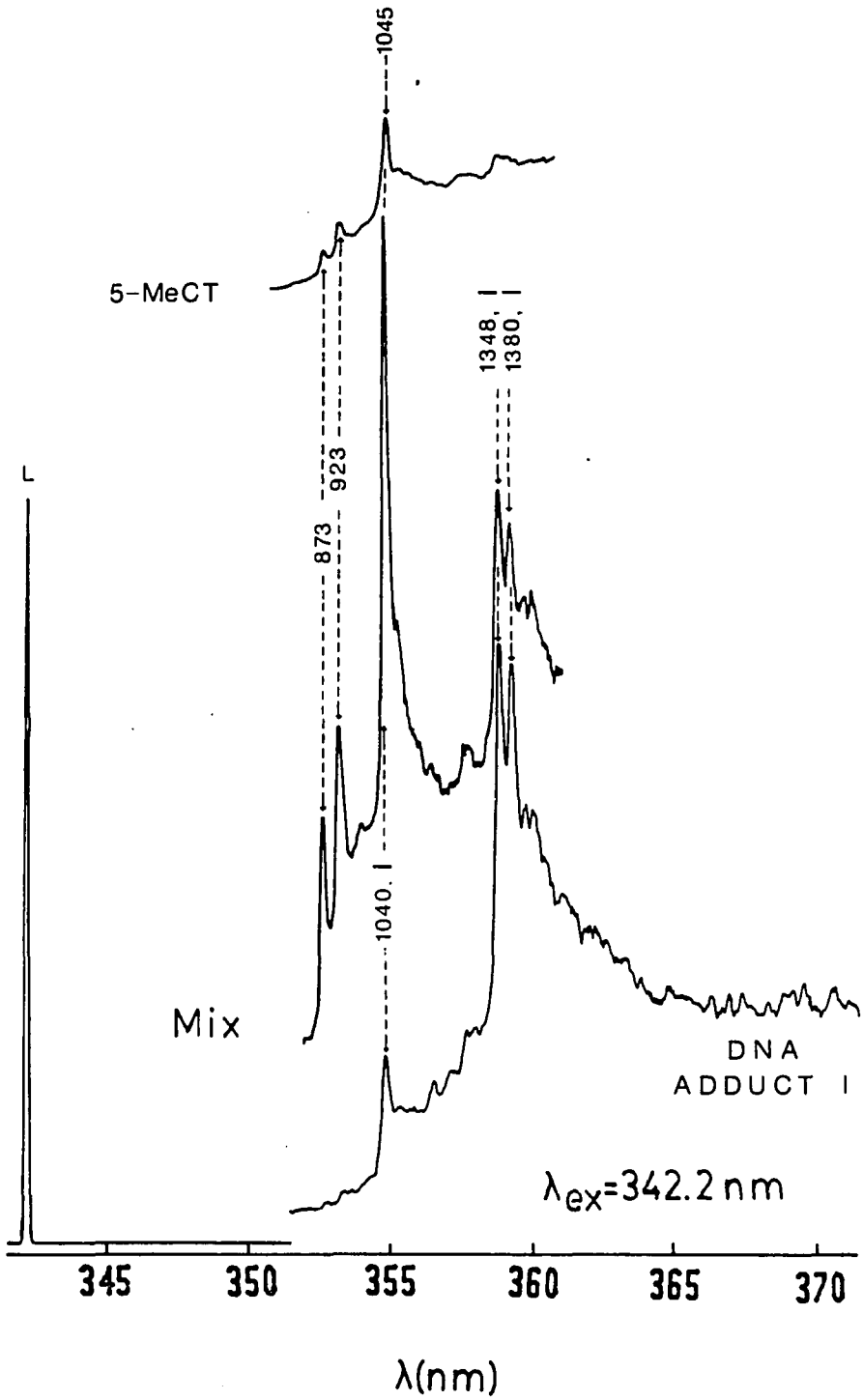
1045
5-MeCT
1348
1380
873
923
L
1040
Mix
DNA
ADDUCT I
λex=342.2nm
345
350
355
360
365
370
λ(nm)

zero-phonon features are labeled with excited-state vibrational frequencies. Both the 5-MeCT and the 5-MeCDE-DNA exhibit weak electron-phonon coupling.

Finally, a complex mixture of all six metabolites and the adducts 5-MeCDE-DNA (I) and B[a]PDE-DNA (III) was analyzed. Resolution by FLN was straightforward when wavelengths (λ_{ex}) were used that provided the best separation of the two adducts from their corresponding tetrols. Some of the results are shown in Figures 18 and 19. For λ_{ex} = 342.2 nm, peaks from three tetrols and 5-MeCDE-DNA are observed, Figure 18. The most important features are labeled with the name of the compound and excited-state vibrational frequencies. When λ_{ex} = 366.1 nm is used, zero-phonon features from the remaining three metabolites are observed, as shown in the lower spectrum of Figure 19. This spectrum was obtained with a PMT detector and without gating. The feature at 1110 cm^{-1}, which is a shoulder riding on the much more intense emission from the B[a]AT-1 tetrol is due to the B[a]PDE-DNA adduct. The parent chromophore of the interfering tetrol is anthracene. The upper spectrum of Figure 19 was obtained with the gateable diode array-OMA system. The fluorescent parent chromophore of the B[a]PDE-DNA adduct is pyrene, Figure 7. Since the lifetime of pyrene is ~ 400 ns (81) and that of anthracene is ~ 5 ns, delay of the gate pulse will lead to a

Figure 18. FLN spectrum of an eight-component mixture including six metabolites and the 5-MeCDE-DNA and B[a]PDE-DNA adducts. L labels the laser peak (λ_{ex} = 342.2 nm), T = 4.2 K. Bands are labeled as 5-MeCDE-DNA, CT, 5-MeCT, and B[a]AT-8 and assigned on the basis of standard spectra for the pure individual compounds

Figure 18

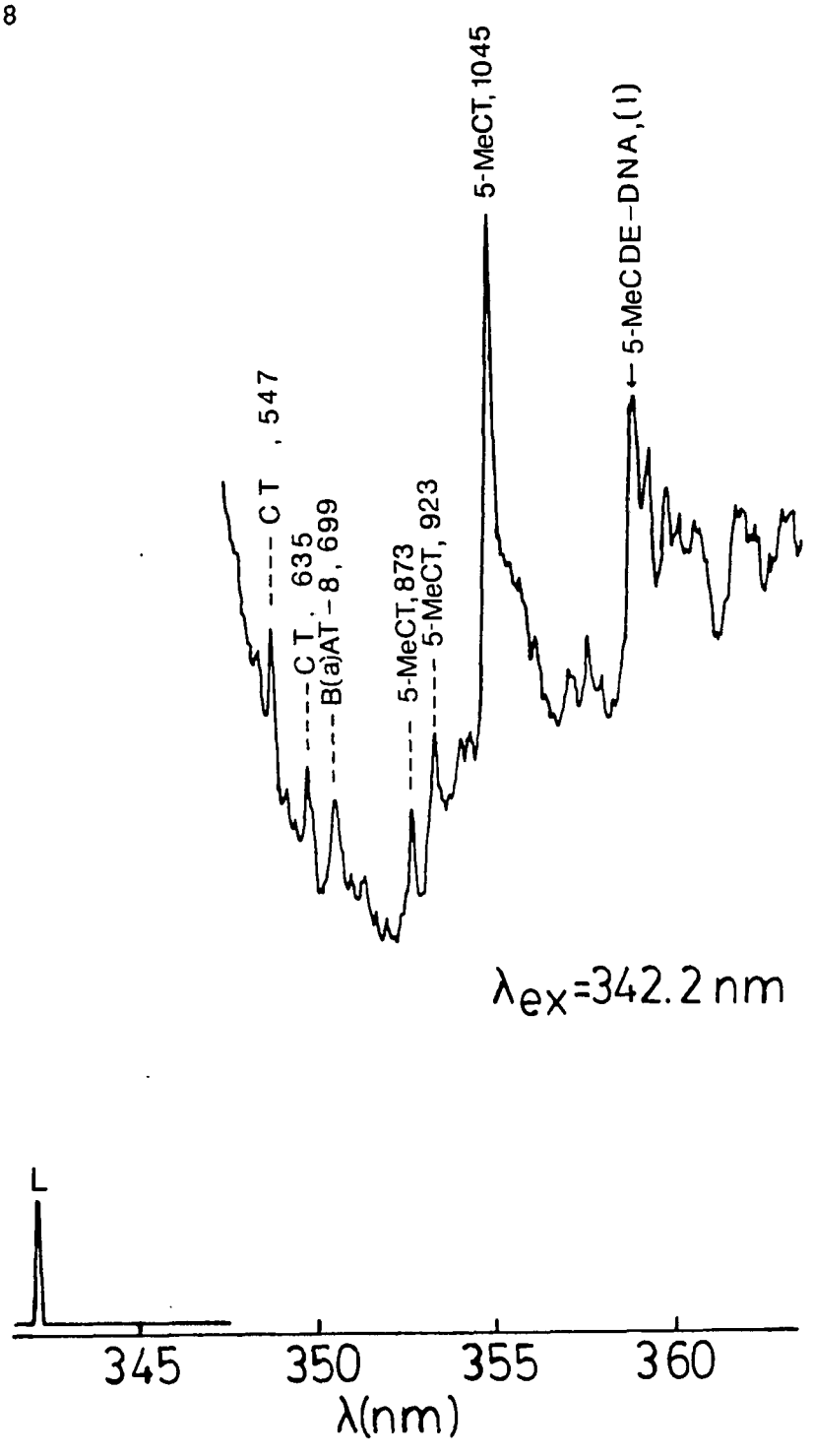
5-MeCT, 1045
← 5-MeCDE-DNA, (I)
---- C T , 547
---- C T , 635
---- B(a)AT - 8, 699
---- 5-MeCT, 873
---- 5-MeCT, 923
λex=342.2 nm
L
345
350
355
360
λ(nm)

Figure 19. FLN spectra of an eight-component mixture (see Figure 18 caption) obtained for excitation wavelength of 366.1 nm. The lower spectrum was obtained ungated with a PMT, and only bands due to three metabolites (B[a]P-diol, B[a]PT, B[a]AT-1) are readily apparent based on standard spectra. The upper spectrum (insert) was obtained with a gateable intensified diode array-OMA (80-ns gate delay) and proves that the weak feature at 1110 cm^{-1} in the lower spectrum is due to the B[a]PDE-DNA (see text)

Figure 19

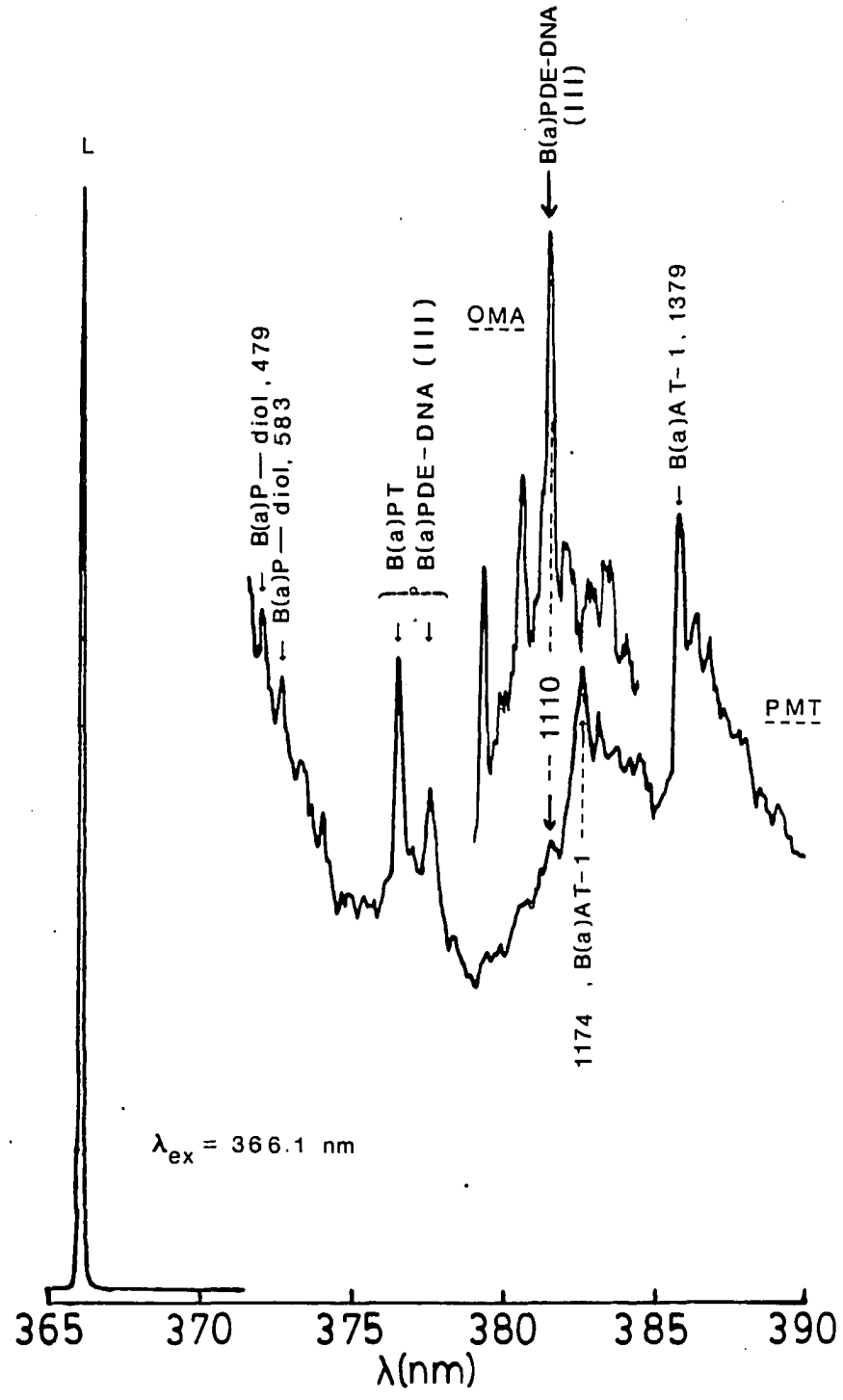
L
B(a)P—diol, 479
B(a)P—diol, 583
B(a)PT
B(a)PDE-DNA (III)
OMA
B(a)PDE-DNA (III)
1110
1174
B(a)AT-1
B(a)AT-1, 1379
PMT
λex = 366.1 nm
365
370
375
380
385
390
λ(nm)

marked reduction of the B[a]AT-1 emission intensity. The upper (inset) spectrum of Figure 19 was obtained with a gate delay of 80 ns, and all features can be assigned to B[a]PDE-DNA. Thus, temporal discrimination greatly enhances the versatility of FLN for analysis of complex DNA-PAH adduct mixtures.

C. Hole Burning Considerations

Turning to the question of detection limits we note that with a conventional prototype FLN system, which employed a low power (~ 2 mW average power) N_2-pumped dye laser, a detection limit for damage of ~ $5{:}10^6$ base pairs for ~ 30 μg of DNA has been reported for the BPDE-DNA adduct at an FLN resolution of ~ 10 cm^{-1} (74). This corresponds to the detection of ~ 1 pmol of the bound metabolite, which is roughly three orders of magnitude too high for practical biological applications. Calculations indicated that the FLN system described in Section II should provide a detection limit of ~ 1 fmol. It should be noted that the $S_1 \leftarrow S_0$ absorption transition of pyrene is weak (ε_{max} ~ 25- at room T in ethanol solution) and that its fluorescence quantum yield is ~ 0.65 (81). For more strongly absorbing and fluorescent chromophores such as the aflatoxins one would anticipate lower detection limits.

Prior to the studies on BPDE-DNA and B[a]P tetrol, the FLN system of Figure 9 was used to determine the detection

limits for the moderately strong fluorescers 1-methylpyrene and anthracene. For both compounds a FLNS detection limit of 1 fmol or ~ 0.2 pg can be achieved at a spectral resolution of ~ 10 cm^{-1}. This value would correspond to the detection and characterization of an equivalent 30 µg DNA sample having a damage level of $1:10^8$ bases. Thus, the FLN system appeared to have the capability to detect and characterize the low DNA damage levels of <u>in vivo</u> biological samples.

As model compounds, B[a]P tetrol and BPDE-DNA were analyzed. Using nondegassed samples, excitation of the pyrene chromophore with sufficiently high laser intensity led to photodegradation and, as a consequence, spectral degradation. Figure 20 shows the effect of photodegradation on the FLN spectrum of a nondegassed B[a]P tetrol sample; the upper curve in Figure 20 is taken with low laser power density (5 mW/cm^2), and the lower curve after scanning the laser through the very broad absorption region ((0-0) band) at high laser power density (~ 600 mW/cm^2). One can clearly see that significant changes have taken place -- the ZPLs have disappeared, leaving only a broad fluorescence background. Warming the sample to room temperature and then cooling to low temperature (4.2 K) did not restore the ZPLs -- the photodegradation was not thermally reversible.

Figure 20. FLN spectrum of B[a]P-tetrol at T = 4.2 K, λ_{ex} = 355.4 nm. Upper curve is taken with low average laser excitation power density, I = 5 mW/cm^2. Lower curve is taken after scanning the laser through the very broad absorption region (0,0) band at high laser power (I = 600 mW/cm^2)

Figure 20

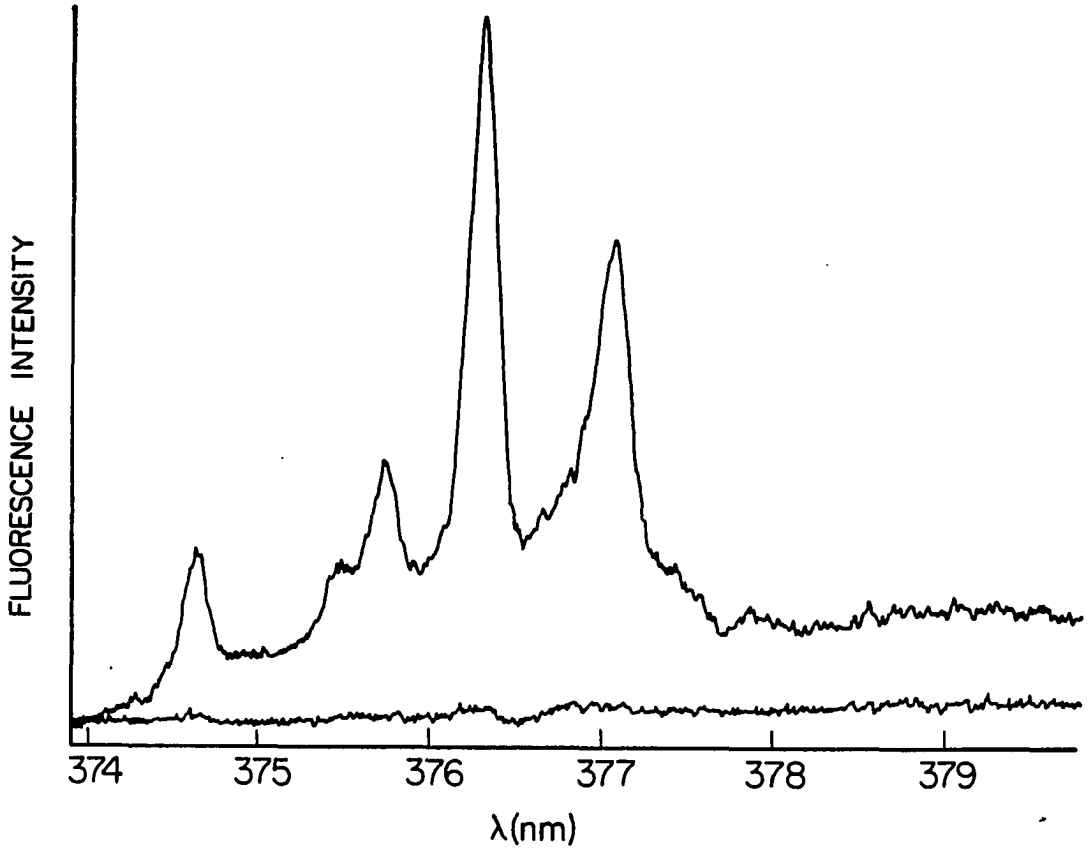

Similar results have been obtained for nondegassed BPDE-DNA samples.

A brief discussion of spectral hole burning is appropriate at this point to better understand the observed photodegradation of the fluorescence signal. There are two types of spectral hole burning: photochemical hole burning (PHB) and non-photochemical hole burning (NPHB). With an understanding of FLN, as presented in section I, PHB follows in a natural way. It is apparent that if the species giving rise to the absorption is photoreactive, isochromat selective photobleaching can occur. Hole burning is based on the ability of matrix-isolated optical absorber to undergo a reaction while in an excited state (82-84). This reaction can be a chemical modification, e.g., irreversible molecular fragmentation, reversible tautomerization or photoionization (in the case of trapped electrons in organic glasses) (82,83). In the case of NPHB the mechanism involves a structural relaxation that changes the physical state of the system (triggered by host two level system (TLS) transitions and/or rearrangement of local host structure) (83). Since these processes lead to a change of the optical transition energy a spectral hole is produced whose width is determined by dephasing processes acting on the molecule under consideration and, at least partly, by time dependent spectral diffusion (85-87). Zero-phonon

Figure 21. Inhomogeneous line broadening and hole burning. (a) Inhomogeneous line broadening and (b) photochemical and nonphotochemical hole burning. Γ_I ~ few hundred cm^{-1} for glasses; Γ_H (homogeneous linewidth) $\leq$ 0.1 cm^{-1} at T ~ 1.5 K for organic molecules in glasses. In (b) (the bottom schematic) the "product" corresponds to new impurity-glass site configurations produced by light induced TLS_{ext} relaxation

Figure 21

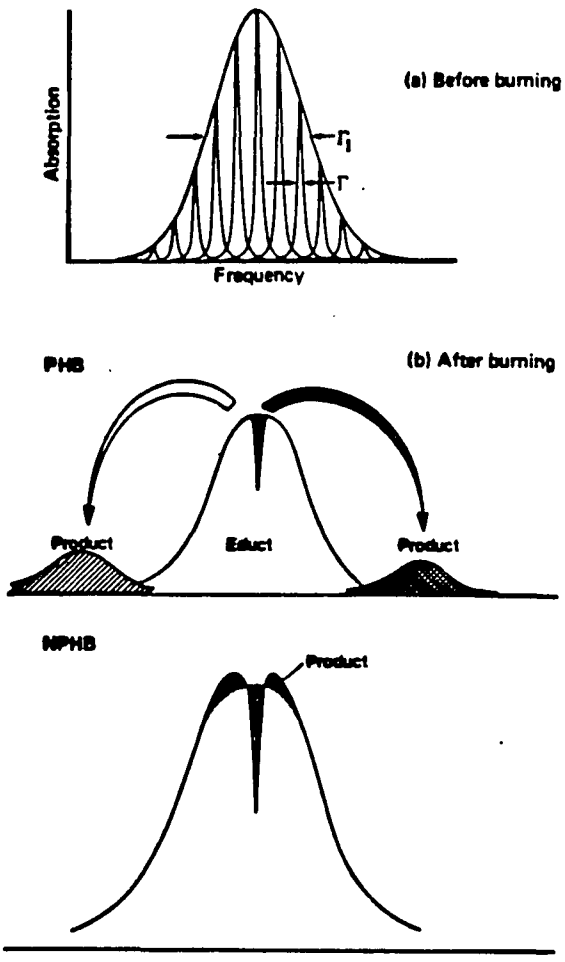
(a) Before burning
Absorption
Frequency
Γ_i
Γ
PHB
(b) After burning
Product
Educt
Product
NPHB
Product

Figure 22. The two-level system (TLS) model for nonphotochemical hole burning. The subscripts α and β label the TLS that interact with the impurity in its ground and excited electronic states. The tunnel frequency, W, depends on the tunnel parameter λ which is defined as $d(2mV)^{1/2}/h$, where m is the tunneling mass. The frequency ω_B is that of the burn laser

Figure 22

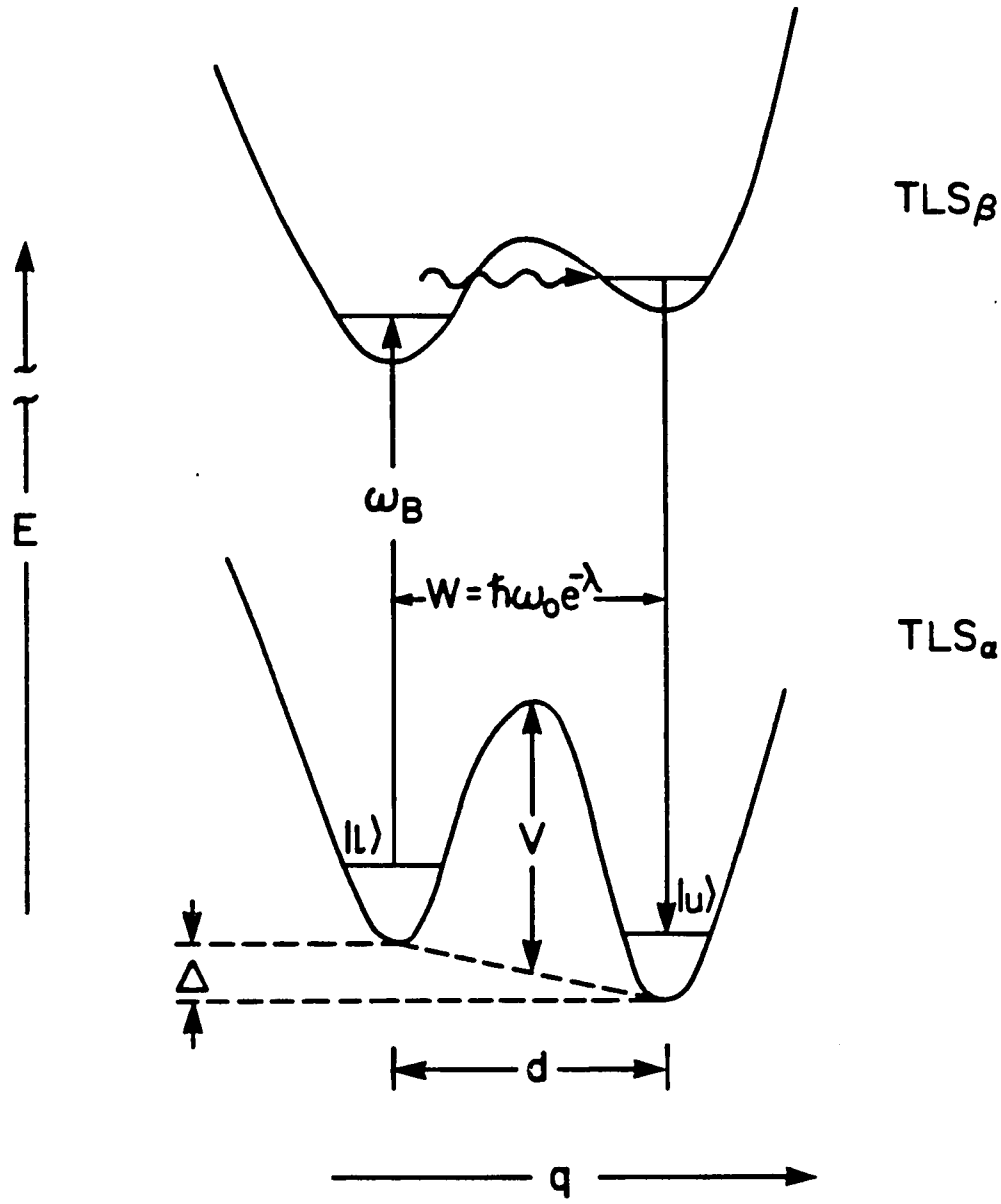
TLS$_\beta$
E
ω_B
$W = \hbar\omega_0 e^{-\lambda}$
TLS$_\alpha$
$|L\rangle$
V
$|u\rangle$
Δ
d
q

holewidths are usually very narrow ($\lesssim$ 0.2 cm^{-1}), and widths as narrow as ~ 100 MHz have been observed at T = 1.5 K (83,84,88).

Photoreactivity is not required in NPHB (82-84); what is required is a host with a "faulty memory" for its pre-excitation configuration near the absorber. That is, upon completion of the cycle from ground state to excited state and back to the ground state, the host configuration must have changed more or less permanently if persistent holes are to be produced (bottom schematic of Fig. 21). With perhaps one or two exceptions, NPHB has only been observed in glasses and polymers. Given the immense disorder which exists in such hosts (89), this restriction is perhaps now not so surprising.

In Figure 22 the simple TLS model for the NPHB mechanism (90) is shown. It approximates the glass bistable configurations with a distribution of asymmetric intermolecular double well potentials (TLS). There is a distribution of barrier heights (V), asymmetries (Δ) and displacements (d), and, of course, there may also be distinctly different intermolecular coordinates, q. From Figure 22, a mechanism for persistent NPHB at T = T_B (burn temperature) becomes apparent if it is postulated that a subset of the distribution of TLS interacting with the impurity has the following properties at T_B: relaxation

between the two minima for the ground state is slow on the time scale of the experiment, while for the excited impurity the relaxation is competitive with the excited state decay. For example, with the frequency ω_B tuned to the "left" optical transition, barrier hopping or tunneling in TLS_β leads to population of the right-well configuration in the ground state. The degree of competitiveness determines the hole burning quantum efficiency (83,84).

Summarizing, the general definition of NPHB is isochromat selective photobleaching due to the production of a glass state which, at T_B, is thermally inaccessible to the original state. For low temperatures NPHB is the result of phonon assisted tunneling of TLS and provides a tangible illustration of TLS relaxation (83,84).

As a first measure to reduce or eliminate spectral hole burning the samples were degassed, as described in the experimental section, to remove oxygen. For degassed samples the spectral degradation is less significant. The results indicate that a significant photodegradation route in nondegassed samples is due to photooxidation. Figure 23 shows the FLN spectrum of a degassed BPDE-DNA sample having a damage level of $8{:}10^7$ bases (curve 1) and a higher modification BPDE-DNA sample (curve 2). The signal/noise ratio of the strongest peak in curve 1 is greater than 20:1, resulting in a detection limit of ~ $1{:}10^7$ bases for

Figure 23. FLN spectra of BPDE-DNA (degassed) with a modification level of 8 adducts in 10^7 bases (curve 1) and a modification level of 1 adduct in 183 DNA bases (curve 2), λ_{ex} = 369.6 nm

Figure 23

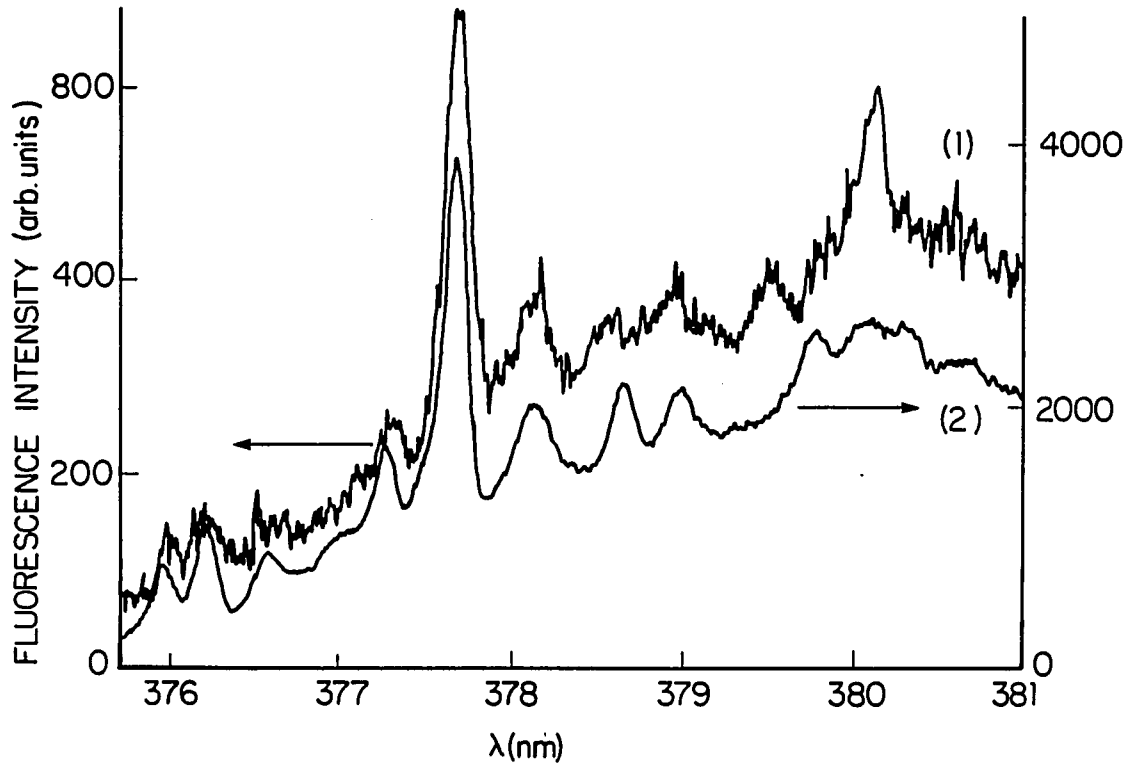
FLUORESCENCE INTENSITY (arb.units)
800
400
200
0
376
377
378
379
380
381
λ(nm)
(1)
(2)
4000
2000
0

BPDE-DNA. For a DNA sample of 30 μg, this corresponds to ~ 10 fmol of adduct detected. This is still an order of magnitude greater than the 1 fmol detection limit mentioned earlier, and, indeed, while the photodegradation due to photooxidation has been eliminated in the degassed samples, an efficient NPHB process is still present, which is responsible for the higher than expected limit of detection.

Figure 24 illustrates the effect of NPHB on the FLN spectrum of degassed BPDE-DNA sample. Figure 24a shows the FLN spectrum at short irradiation time and low laser power density (85 mW/cm^2). Spectral hole burning was then carried out with high laser power density (400 mW/cm^2), and Figure 24b shows the decrease of the intensity of the strongest ZPL ((0-0) site at ω = 579 cm^{-1}) as a function of irradiation time. The fluorescence spectrum after hole burning is shown in Figure 24c, where one can readily observe that the ZPLs have been eliminated.

Non-photochemical hole burning <u>is</u> a thermally reversible process, that is, by simply warming the sample to room temperature the holes in the absorption profile are "refilled" and the absorption spectrum returns to its original form. However, during the actual experiment, NPHB reduces both the selectivity and sensitivity of the FLNS method. The sharpness of the ZPLs disappears due to the photobleaching of the sites which have their zero-phonon

Figure 24. Effect of NPHB as a function of laser power density and time. a) FLN spectrum of BPDE-DNA (degassed). Excitation laser power density I = 85 mW/cm^2, λ_{ex} = 369.6 nm. The numbers correspond to excited state vibrations (in cm^{-1})

b) Decay of the integrated fluorescence intensity of the 579 cm^{-1} peak (Fig. 24a) for a laser excitation power density of 400 mW/cm^2

c) Resulting FLN spectrum after burning (at 400 mW/cm^2) for 30 min. The experimental conditions are as in Fig. 24a

Figure 24

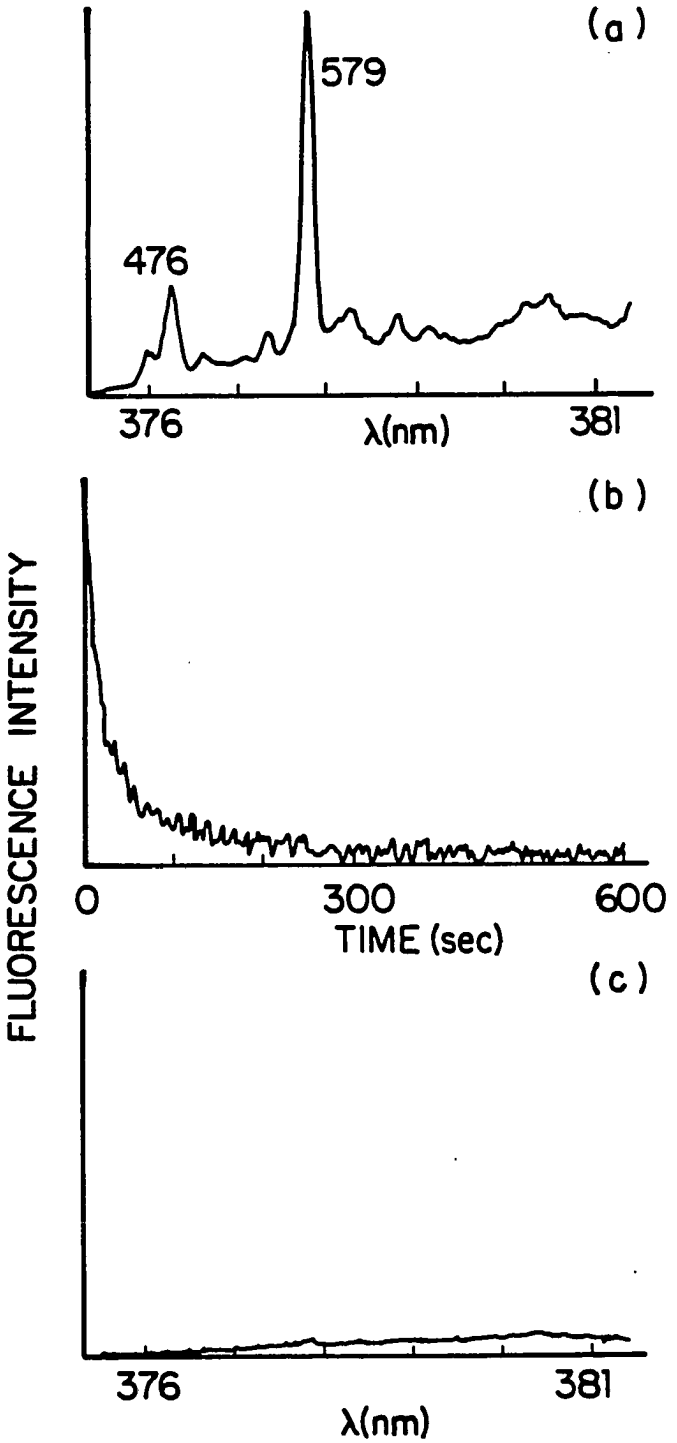
(a)
579
476
376
λ(nm)
381
(b)
FLUORESCENCE INTENSITY
0
300
600
TIME (sec)
(c)
376
381
λ(nm)

transition at the laser frequency, so the characteristic FLN fingerprint of the molecule under study is eventually destroyed. Also, since the NPHB process removes some of the absorbers from their initial position within the absorption profile (at the laser frequency), the fluorescence intensity necessarily decreases. This is particularly troublesome when one wants to measure very small fluorescence signals from low concentration (~ 1 fmol) samples, since in those cases it is necessary to use high laser excitation power densities to detect any fluorescence, but the high power densities also accelerate the NPHB process. Thus, in order to improve the limits of detection for BPDE-DNA (and other samples in which NPHB occurs), methods of reducing NPHB were necessary.

As discussed earlier, line-narrowed spectra can be obtained by exciting either the origin or vibronic transitions of a given molecule. In the presence of NPHB, vibronic excitation is preferable for $T \lesssim 4$ K. This is true because the homogeneous vibronic linewidths, Γ_v, are much broader than the origin linewidth (mainly due to rapid vibrational relaxation of the vibronic levels). Therefore, vibronic excitation allows one to use excitation power densities of roughly an order of magnitude higher (compared to those used for origin excitation) before optical saturation of the transition occurs.

As Figure 24 clearly demonstrates, though, excitation into the vibronic region of the absorption profile does not sufficiently reduce NPHB in BPDE-DNA samples, so other methods of decreasing the photobleaching were sought. Simultaneously scanning λ_{ex} and the observation wavelength (λ_{obs}) at a constant energy separation reduces the NPHB process by limiting the time that each isochromat is exposed to the laser. The spectra obtained indicate that this procedure does not distort the shape of the FLN spectra (at least for scans of ~ 50 cm^{-1} or less) and that the fluorescence intensity is increased. The depletion of the ground state population can be decreased by subjecting the sample to high intensity white light pulses. This procedure decreases the NPHB effects and thus increases fluorescence (91). In addition, the theory of dispersive kinetics and experimental results indicate that the quantum efficiency for hole burning decreases at higher temperature (84), so another way to decrease the NPHB process is to perform the FLNS experiments at temperatures of ~ 10-30 K.

The preceding discussion indicates that combining vibronic (1,0) excitation, simultaneous scanning, white light restoration pulses, and using a temperature slightly higher than 4.2 K should enable a lower FLNS limit of detection for BPDE-DNA to be realized. Indeed, this is the case, as is shown in Figure 25. Vibronic excitation is

Figure 25. FLN spectrum of BPDE-DNA (degassed) with a modification level of $8{:}10^{7}$ synchronously scanning λ_{ex} and λ_{obs} over 40 cm^{-1} and using white light restoration pulses (see text) at T = 20 K, (I = 450 mW/cm^{2}). Signal/noise ratio of the most intense peak is greater than 80. Note that the bottom axis is in cm^{-1}, which represents the frequency separation between the laser and the observed fluorescence

Figure 25

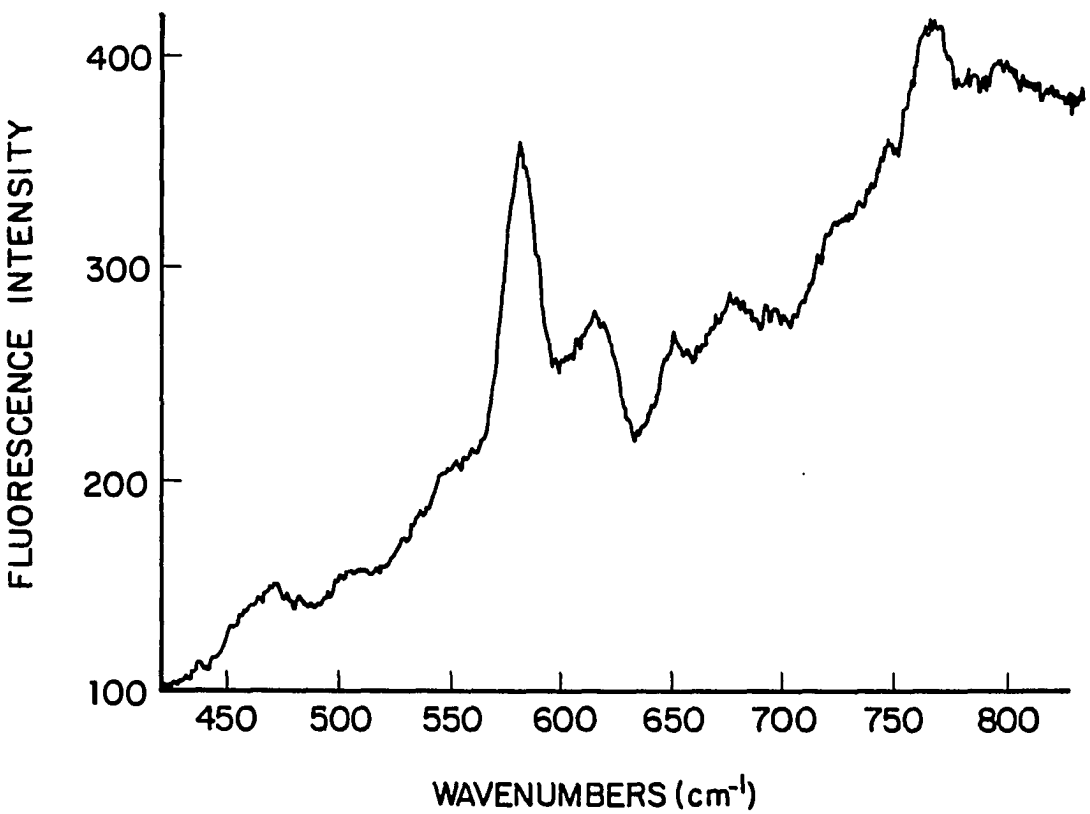
FLUORESCENCE INTENSITY
400
300
200
100
450
500
550
600
650
700
750
800
WAVENUMBERS (cm-1)

employed, and the laser and monochromator have been synchronously scanned over ~ 40 cm^{-1}. One msec white light restoration pulses, delayed 1 msec after the laser excitation pulse have also been used, and the spectrum obtained at T = 20 K. The signal/noise ratio of the strongest peak in Figure 25 is greater than 80, so a limit of detection of ~ 3 adducts:10^8 bases, for a 20 μg DNA sample, is obtained. This corresponds to ~ 2 fmol of adduct detected and illustrates that FLNS does have the requisite sensitivity to analyze and characterize the typically low DNA damage levels of biological samples.

In the presence of the NPHB process, the selectivity of the FLN spectra depends on the exposure time. Therefore, to increase the selectivity, a new analytical approach which combines FLNS with the NPHB process was developed. It is an extension of the procedure used by Bogner and Schwarz (92) and Fünfschilling et al. (93) to describe the correct shape of phonon wings and the electron-phonon coupling. In contrast to ref. 92 and 93, for the reasons discussed above is used.

In the standard FLNS method the zero-phonon site selection is not perfect, i.e., a significant fraction of the fluorescing molecules are excited through phonon wing absorption. The resulting fluorescence spectrum consists of narrow ZPL and broad-band fluorescence arising from various

phonon contributions, depending on the electron-phonon coupling strength (62). Ideally one would like to observe only the spectrum of the molecules which have their zero-phonon transition at the laser frequency and avoid the broad-band phonon fluorescence. To get better selection, therefore, one has to measure an FLN spectrum "A" and then after a given irradiation time (after hole-burning), measure the next spectrum "B". Then the "difference" fluorescence spectrum "A" - "B", representing the FLN spectrum shows very sharp ZPL with their real phonon wings (at least for short burning times to avoid saturation effects), thus increasing the selectivity of the standard FLNS method. These results are presented in Figure 26a, b and c for BPDE-DNA. The most important feature of the above procedure is the fact that one can use much higher laser intensities (to increase fluorescence intensity) and, although the spectra "A" and "B" are broader with less pronounced ZPL, the difference spectrum will always show a sharp fingerprint of the molecules under study, provided that all molecules excited at λ_{ex} through their ZPL have not been totally burned out. This selective difference spectra technique can also be applied to short-lived fluorescing species, where gated fluorescence detection is not available and/or scattered laser light contributes to the signal. The FLN and difference spectra for 6-MeB[a]P are presented in Figure 27.

Figure 26. FLN spectra of BPDE-DNA, λ_{ex} = 369.6 nm
a) Spectrum obtained with a laser excitation power density, I = 85 mΔ/cm^2 and an exposure time of ~ 100 sec
b) Spectrum obtained under experimental conditions as in (a), following a 100 sec exposure to 400 mW/cm^2 excitation power density
c) The "difference" spectrum ((a) - (b)) obtained, as discussed in detail in the text. The numbers correspond to excited state vibrations in cm^{-1} (see Table 4)

Figure 26

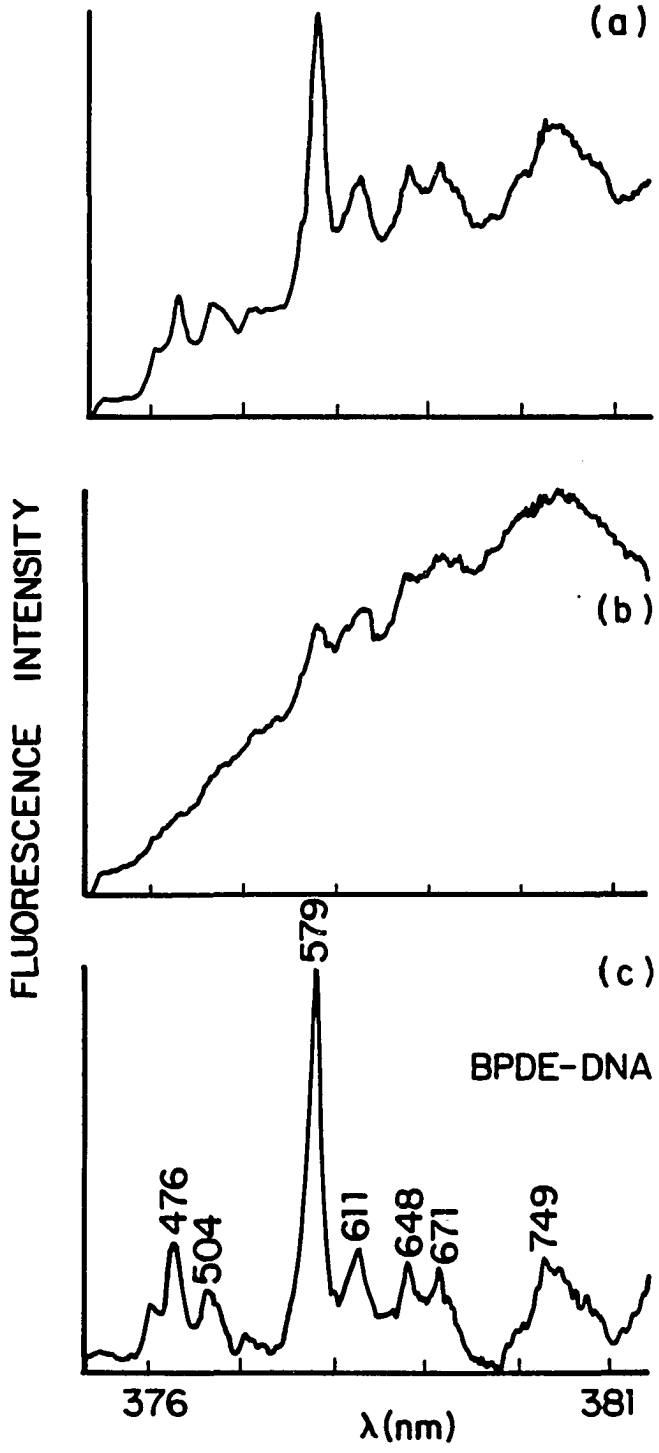
(a)
(b)
(c)
BPDE-DNA
FLUORESCENCE INTENSITY
579
476
504
611
648
671
749
376
381
λ(nm)

Figure 27. FLN spectra of 6-MeB[a]P, λ_{ex} = 388 nm

a) Laser excitation power density, I = 80 mW/cm^2

b) Identical conditions to (a) after several minutes of continuous irradiation with the same laser power density, I = 80 mW/cm^2

c) The "difference" spectrum showing the useful analytical peaks labeled in cm^{-1}

Figure 27

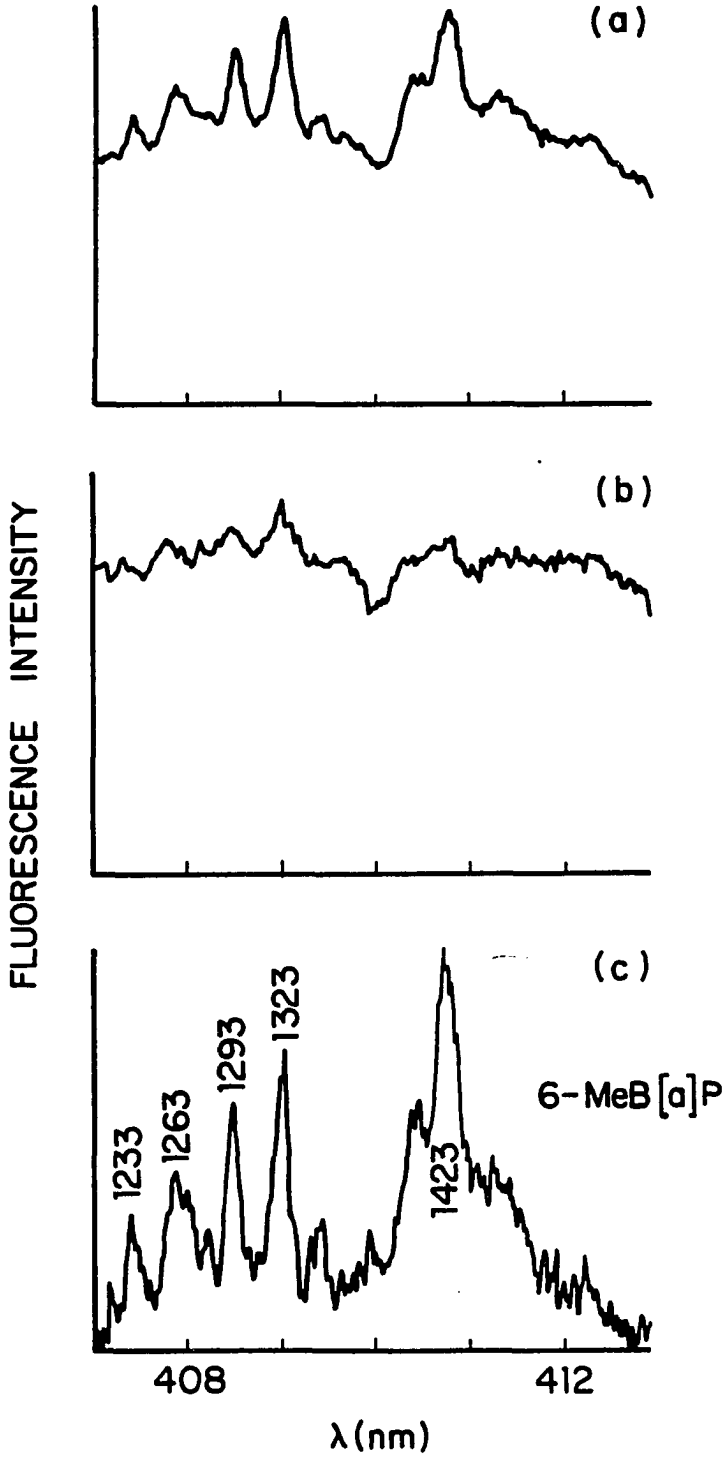
(a)
(b)
(c)
FLUORESCENCE INTENSITY
1233
1263
1293
1323
1423
6-MeB[a]P
408
412
λ(nm)

The spectra were recorded in the continuous mode (not gated) of the OMA system, and the high scattered laser background is virtually eliminated in the difference spectrum.

The spectral subtraction method takes advantage of the fact that the broad-band fluorescence arising from the various phonon contributions is difficult to bleach (for those cases in which the electron-phonon coupling is weak) and is, therefore, fairly consistent. By taking consecutive spectra and subtracting the second from the first, the relatively constant phonon contribution to the fluorescence spectrum is eliminated, leaving sharp ZPLs in the difference spectrum. Thus the constructive use of NPHB in FLNS experiments significantly increases the FLNS selectivity, and is therefore a potentially powerful technique. Detectability is also improved since higher laser power densities can be used, increasing the fluorescence intensity.

D. Applications

1. BPDE-globin adducts

In addition to the detection of DNA-adducts, the high selectivity and detectability of FLNS is applicable for the analysis of globin-carcinogenic metabolite adducts. One example is BPDE-globin, in which BPDE is covalently bound to globin. Figure 28 presents spectra of BPDE-globin excited

Figure 28. FLN spectra of BPDE-globin excited in the (1-0) band: A) λ_{ex} = 369.6 nm and B) λ_{ex} = 368.6 nm. The numbers correspond to the excited state vibrations, in cm^{-1} (see Table 5)

Figure 28

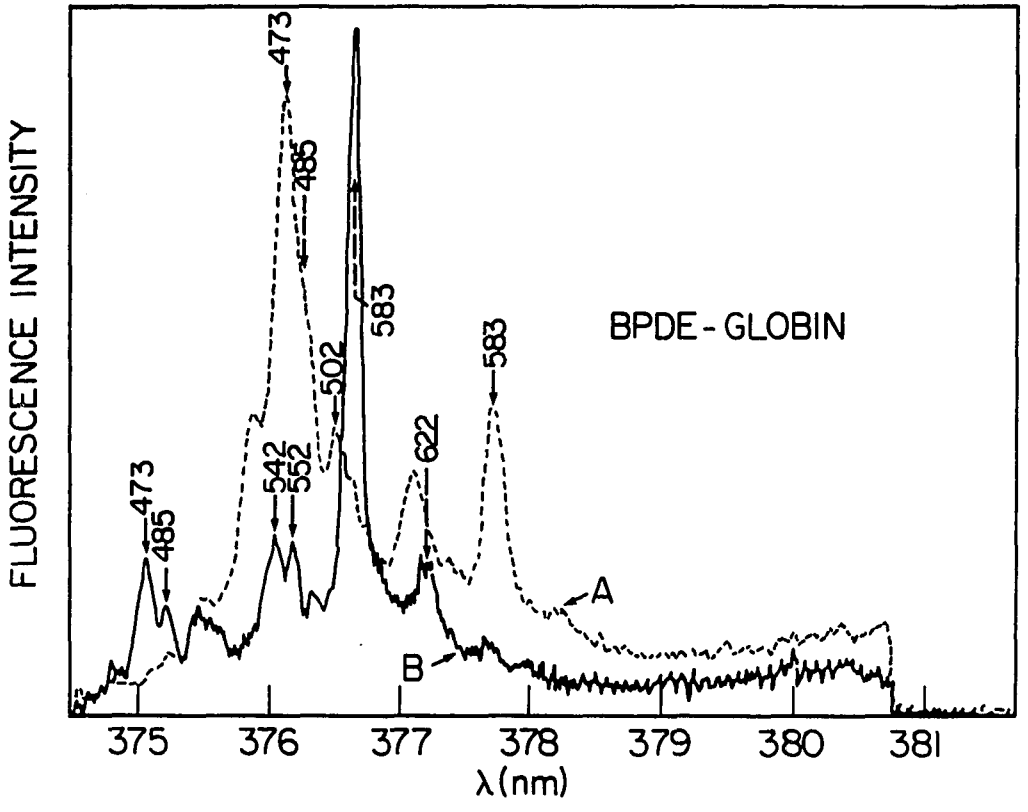
FLUORESCENCE INTENSITY
BPDE - GLOBIN
473
485
542
552
502
583
622
583
485
473
A
B
375
376
377
378
379
380
381
λ(nm)

Table 5. The ground and excited state vibrational frequencies (cm^{-1}) of BPDE-globin in polar glass at T = 4.2 K

BPDE-Globin			
Ground State Vibrations (cm^{-1}) (λ_{ex} = 377 nm)		Excited State Vibrations (cm^{-1})	
341	m	347	(1)
360	w	381	(1)
425	w	409	(1)
464	m	457	(1)
688	w	473	(1,2,3)
760	w	485	(2,3)
786	s	502	(2)
821	w	542	(3)
845	s	552	(3)
909	m	583	(2,3,4)
968	w	622	(3,4)
977	w	653	(4)
1047	w	675	(4)
1113	m	720	(5)
1176	w	745	(4,5)
1246	m	764	(4,5,6)
1411	s	833	(5,6,7)
1558	m	894	(6,7)
1593	w	960	(6,7)
1633	w	1021	(7)
		1028	(7)
		1049	(7)
		1114	(7)

Excited state vibrational frequencies greater than ~ 1200 cm^{-1} were not measured. Excited state vibrational frequencies are dependent on λ_{ex}.

(1): λ_{ex} = 371.5 nm
(2): λ_{ex} = 369.6 nm
(3): λ_{ex} = 368.6 nm
(4): λ_{ex} = 367.2 nm
(5): λ_{ex} = 365.8 nm
(6): λ_{ex} = 364.3 nm
(7): λ_{ex} = 362.9 nm

in the region of the vibronic sidebands of the $S_1 \leftarrow S_0$ electronic absorption band. All the fluorescence peaks correspond to (0-0) transitions, and the peaks follow the shift of the excitation frequency within the inhomogeneous band. The numbers (in cm^{-1}) indicate the vibronic frequencies of the molecule in the excited electronic state (S_1). Table 5 lists the ground and excited state vibrational frequencies, e.g., the fluorescence lines which are sufficiently intense to be useful in the identification of this adduct in a complex mixture. The detection limit for BPDE-globin can be expected to be comparable to that discussed above for BPDE-DNA.

This example shows that FLNS is useful for the direct analysis of polar metabolites responsible for globin damage resulting from covalent binding of the same metabolites which damage DNA. This is significant because there appears to be a correlation between DNA damage and globin damage (94). Since a globin sample is far easier to obtain (than a DNA sample), the analysis of globin-adducts is an attractive alternative to the analysis of DNA-adducts.

2. Metabolites in urine

FLNS is also useful for the direct analysis of polar metabolites in urine. The analysis of mutagens in urine is generally complicated by several factors: urinary metabolites are usually present in low concentration and,

for fluorescence-based techniques, urine contains a variety of compounds which fluoresce. The selectivity and detection powers of FLNS and the possibility of time resolution should, in many cases, successfully overcome these difficulties.

Figure 29 shows the FLN spectra of B[a]P tetrol in a 1:1 urine:pure glass mixture, "urine glass." The spectrum in Figure 29a was obtained using vibronic excitation and, therefore, the labeled peaks (in cm^{-1}) correspond to excited state vibrations. The spectrum in Figure 29b was acquired with origin excitation and, therefore, its peaks correspond to ground-state vibrations. Comparison of the vibrational frequencies found in Figure 29b with those listed in Table 2 for B[a]P tetrol in pure glass shows that there is a good agreement.

For B[a]P tetrol in urine a ~ 1 picomole limit of detection has been obtained; further lowering of this limit is hampered by the presence of many other fluorescing compounds present in urine, which yield a relatively strong and broad background. A simple sample cleanup procedure could be used to remove these interfering compounds, resulting in a lower detection limit. Such a procedure would probably involve either an extraction with a nonpolar solvent or preconcentration on a disposable chromatographic column.

Figure 29. FLN spectra of B[a]P tetrol in "urine glass" a) Spectrum obtained with (1-0) excitation (λ_{ex} = 369.6 nm). The labeled peaks correspond to excited state vibrational frequencies, in cm^{-1} b) Spectrum obtained with (0-0) excitation (λ_{ex} = 377.1 nm). The labeled peaks correspond to ground state vibrational frequencies, in cm^{-1}

Figure 29

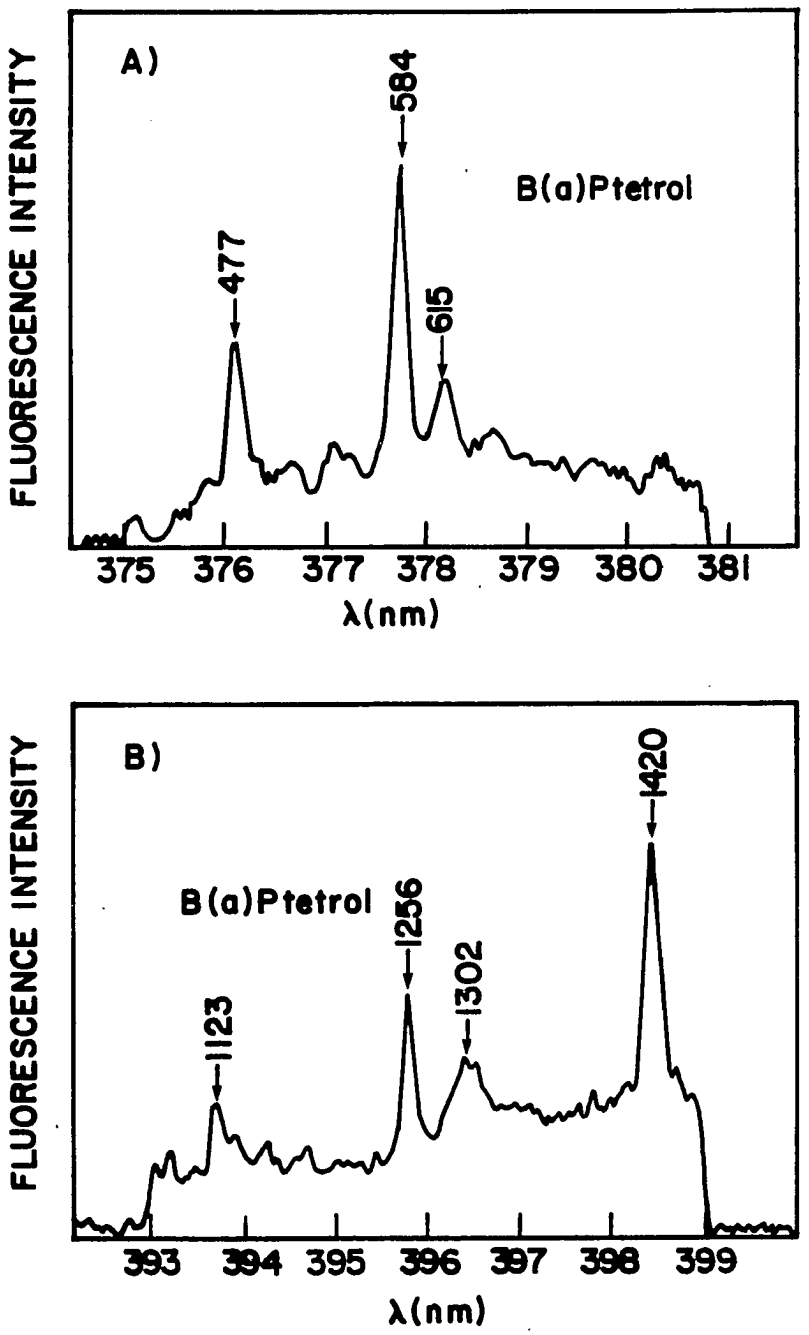
A)
584
B(a)Ptetrol
477
615
FLUORESCENCE INTENSITY
375 376 377 378 379 380 381
λ(nm)
B)
1420
B(a)Ptetrol
1256
1302
1123
FLUORESCENCE INTENSITY
393 394 395 396 397 398 399
λ(nm)

Other B[a]P metabolites, such as 7-HTHB[a]P, 10-HTHB[a]P, B[a]P-diol and THB[a]P have been analyzed. In all these cases and many others (61-64,66,69,72-74) FLN spectra are obtainable, illustrating that FLNS is a widely applicable technique for the analysis of fluorescing compounds. Thus FLNS is a useful technique for monitoring a large number of environmental mutagens and carcinogens to which humans are exposed. Although the analysis of urinary metabolites does not provide a direct measure of the damage due to these compounds, it does provide a convenient indicator of human exposure since many mutagenic and carcinogenic metabolites and elimination products, e.g., detoxification and DNA adduct repair products, are excreted in urine.

3. Real samples

FLNS was successfully applied to the DNA isolated from fish exposed under controlled laboratory conditions to water contaminated with a mixture of dibenz[a,h]anthracene, benzo[b]fluoranthene and benzo[a]pyrene. The sample was expected to have a DNA damage level $<< 1{:}10^6$ from any single metabolite. Analysis by the Randerath (39,40) procedure had proven unsuccessful. Figure 30 shows the FLN spectrum, obtained under the conditions suitable for determination of the BPDE-DNA adduct resulting from a metabolite of benzo[a]pyrene. The fish FLN spectrum, however, does not

Figure 30. FLN spectrum of fish DNA, λ_{ex} = 369.6 nm (see discussion in text)

Figure 30

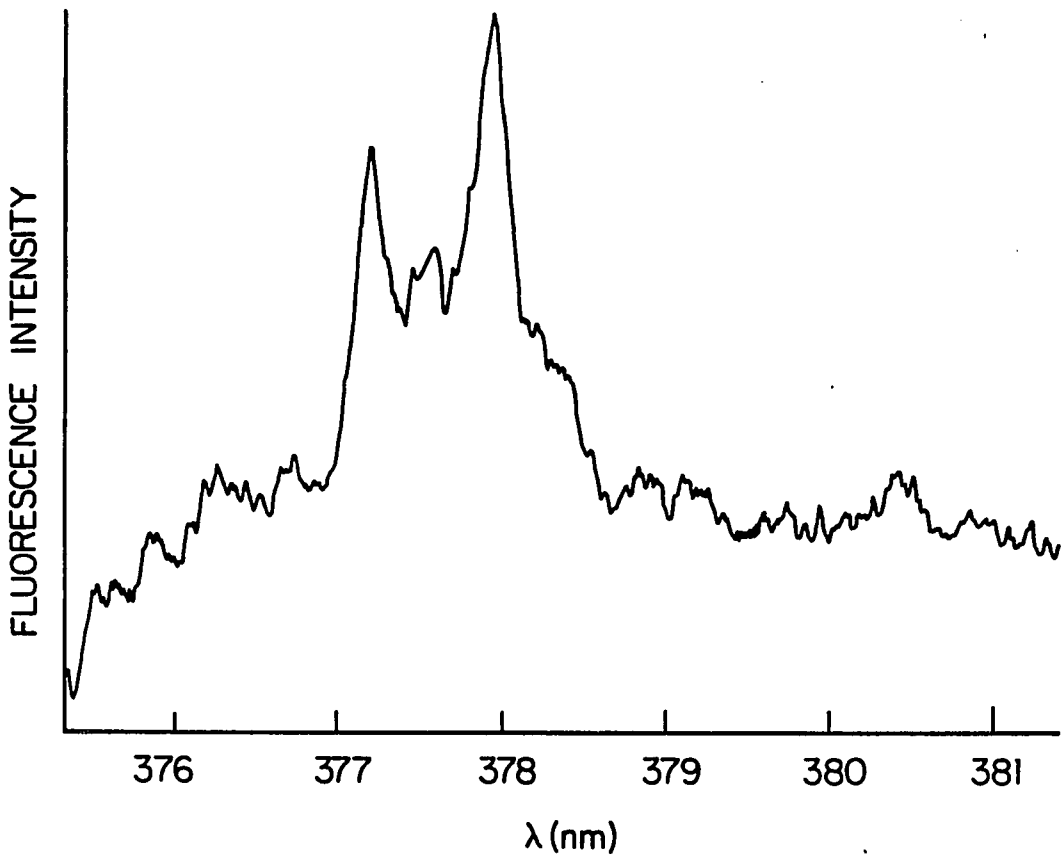

match the BPDE-DNA standard spectrum (compare Figs. 23 and 30). Although a small contribution from the BPDE-DNA adduct is possible, FLN contributions from other species (as yet unidentified) dominate the spectrum. In addition it is possible that the BPDE metabolite can assume more than one binding conformation with DNA. The probability distribution function for binding could be affected by the mode of DNA exposure and other factors. It should be noted that the fluorescence spectra of the standard BPDE-DNA adduct and the fish DNA would be indistinguishable when obtained under non-line narrowing conditions.

Further studies designed to characterize the species that are contributing to the fish DNA FLN spectrum were hampered by the unavailability of standard DNA adducts for the other two species involved. It is the author's belief that upon receipt and analysis of these standard adducts the specie or species responsible for the spectrum in Figure 30 will be identified.

4. Metabolic pathways

Preliminary FLN results in the study of one electron oxidation as a metabolic pathway in the binding of B[a]P to DNA have been obtained. By this pathway, as described in the introduction, it is believed that B[a]P is oxidized to a radical cation at the 6 position which can bind to the slightly nucleophilic DNA. It is further postulated that

this binding mainly occurs at the N-7 and C-8 positions of guanine bases in the DNA chain. Following adduction the adducted bases are thought to depurinate, the N-7 bound adducts depurinating at a much faster rate than the C-8 bound adducts (see Figure 8 and reference 32). These preliminary FLN experiments were concerned with detecting these depurination products in DNA samples exposed to B[a]P in the presence of horseradish peroxidase and H_2O_2 (HRP-DNA). The main depurination products expected are B[a]P-C-8dG, B[a]P-C-8gua, and B[a]P-N-7gua (32). For these studies, however, due to the rapid depurination rate of B[a]P-N-7gua and the necessary DNA cleanup procedure to remove excess B[a]P, the HRP-DNA samples are expected to contain only trace amounts of this base adduct. Samples of B[a]P-C-8dG, B[a]P-C-8G, B[a]P-C-8gua, B[a]P-N-7gua, 6-MeB[a]P, and B[a]P were obtained and characterized at several excitation and observation wavelengths. Resolution of B[a]P, 6-MeB[a]P, and B[a]P-N-7gua from each other and the rest of the base adducts was trivial. The spectra obtained for B[a]P-C-8dG, B[a]P-C-8G, and B[a]P-C-8gua were very similar at the excitation wavelengths employed. This is not surprising when one notes that these base adducts are the depurination products from the same DNA adduct with only small structural differences, as shown in Figure 8. Figure 31 shows the spectra of B[a]P-C-8gua, B[a]P, and two HRP-DNA

Figure 31. FLN spectra of B[a]P-C-8gua, B[a]P, and two HRP-DNA samples, HRP-DNA (1) and HRP-DNA (3). The HRP-DNA (1) sample has undergone a more extensive cleanup procedure to remove excess B[a]P. See text

Figure 31

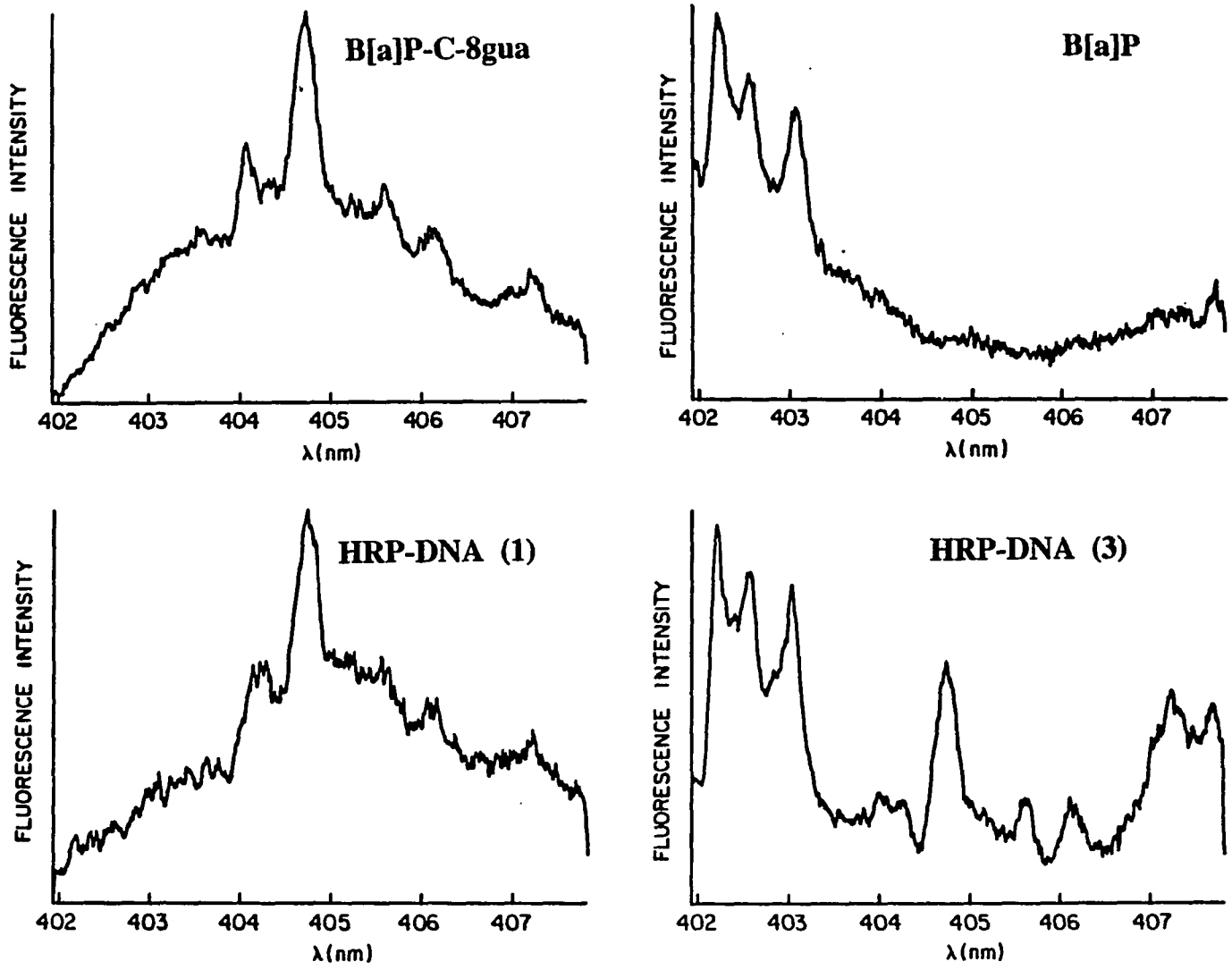
B[a]P-C-8gua
B[a]P
HRP-DNA (1)
HRP-DNA (3)
FLUORESCENCE INTENSITY
λ(nm)
402
403
404
405
406
407

samples differing in the extent of post reaction cleanup, HRP-DNA having the more extensive cleanup. It is obvious that the HRP-DNA spectrum arises from the addition of the B[a]P and B[a]P-C-8gua spectra, while the HRP-DNA spectrum is missing the features associated with B[a]P. Due to the similarities of the three C-8 bound adducts it could not be conclusively determined which of these adducts are responsible for the features in the HRP-DNA spectrum. It should be emphasized that the data presented here are preliminary, further experiments are underway to resolve all of the adducts and identify the species present in the HRP DNA samples. The details and results of these and future experiments will be found in the thesis of Dan Zamzow, graduate student, Iowa State University. The important conclusion that should be drawn from these initial results is that FLNS is directly applicable to the investigation of metabolic pathways in chemical carcinogenesis.

IV. CONCLUSIONS

The basic thrust of this research was to develop a prototype FLN system (69) into a highly selective and sensitive state of the art system for the detection and resolution of the PAH metabolites and adducts encountered in chemical carcinogenesis.

The selectivity of FLNS was demonstrated by the successful resolution of separate mixtures of six polar PAH metabolites, five intact DNA adducts, each PAH metabolite and its corresponding DNA adduct, and finally six PAH metabolites and two DNA adducts. As employed for these complex mixtures, the selectivity is derived from the FLN phenomenon itself, selective excitation, time resolution, and vibronic excitation.

To demonstrate the sensitivity of FLNS, the often-studied BPDE-DNA adduct was used as a model. A detection limit of ~ 3 modified bases in 10^8 was determined using 20 μg of DNA, which corresponds to ~ 1 femtomole of adduct. In obtaining this detection limit for the bound metabolite at a spectral resolution of ~ 8 cm^{-1} it was necessary to eliminate the effects of photooxidation and NPHB which were both detrimental to the observed fluorescence intensity when the necessary high excitation power densities were employed. The elimination of photooxidation was trivial and was accomplished through the use of anaerobic sample conditions.

Circumventing the effects of NPHB was of a more challenging nature and required synchronous scanning of the laser and monochromator together with white light restoration pulses and higher sample temperatures. The first, synchronous scanning, was used to minimize radiation exposure of each isochromat and the last two were used to facilitate spectral diffusion/hole filling, all led to increased fluorescence intensity.

The broad applicability of FLNS in chemical carcinogenesis is demonstrated through its application to globin adducts, polar metabolites in urine, real samples, and the investigation of metabolic pathways. Moreover, FLN is operative for heme proteins (95) and photosynthetic antenna protein complexes (96). The point is that FLNS will be applicable to a wide range of biomolecules and biomolecular problems.

In addition to being highly selective, highly sensitive, and versatile, FLN spectrometry is a practical technique. For a laser-based method the technology is simple (components available commercially) and the procedure for rapid sample cool-down (~ 2 minutes) insures a sample turnover rate that is high. Each spectrum presented here was acquired on average in about 5 minutes. Thus, when the optimum excitation wavelengths for species of interest are known, dozens of samples can be analyzed during the course

of a day. At the same time, spectral features due to unknown components in a mixture would be identified.

The introduction of this dissertation highlighted the characteristics of an "ideal" analytical method for the study of chemical carcinogenesis, and presented the most promising techniques. None of those presented possessed all of the desired characteristics. FLNS, however, most closely matched these requirements, its main limitation being the necessity of a fluorescing species of interest. This is not a great limitation in light of the fact that the two most potent classes of chemical carcinogens, Aflatoxins and PAH (97), are composed of strongly fluorescing compounds.

To summarize, FLNS is a rapid, broadly applicable, highly sensitive, and highly selective analytical technique that can directly analyze carcinogenic metabolites and intact DNA adducts with minimal sample preparation. For these reasons FLNS should play an important part in the future investigation of chemical carcinogenesis.

Future research with FLNS should include the continued investigation of one-electron oxidation as a metabolic route for the formation of PAH-DNA adducts. These studies should include the characterization of a large number of synthesized nucleoside and DNA adducts in order to build a spectral library of adducts. With this information the rapid identification of unknown adducts present in real

samples would be possible, yielding evidence of the metabolic process involved.

FLNS studies to determine the relationship between carcinogenic exposure and metabolite levels in urine should also be pursued, along with similar studies involving globin adducts in blood. A successful outcome of these studies would establish FLNS as a suitable method for the routine monitoring of carcinogen exposure in the workplace.

Finally, FLNS should be applied to the study of the aflatoxins. The aflatoxins are the most potent naturally occurring chemical carcinogens (98), and can be present in peanuts, peanut butter, milk and grain. Presently there is no adequate method for screening foods for these compounds. Initial experiments from this laboratory, not presented here, indicate that FLNS may be able to sensitively and selectively determine these compounds. If so, FLNS could be used to investigate aflatoxin DNA adduct metabolism, and it could also be employed as a method to screen foodstuffs for these deadly carcinogens.

Clearly, FLNS has the potential to be an important analytical tool for the investigation of many biological applications. It is the author's opinion that the most exciting area of research with FLNS is its application to

the investigation of metabolic pathways in chemical carcinogenesis. It is this area which should, and undoubtedly will, receive the most attention in future work from this laboratory.

V. LITERATURE CITED

1. Levin, D. L.; Devesa, S. S.; Goodwin, J. D.; II, Silverman, D. T. Cancer Rates and Risks 2nd ed., U.S. Government Printing Office: Washington, D.C., 1974; Section 1.

2. The Cell Cycle and Cancer; Baserga, R., Ed.; Marcel Dekker, Inc.: New York, New York, 1971; Vol. 1.

3. Hieger, I. Carcinogenesis; Academic Press: New York, 1961; pp. 7-17.

4. Pott, P. Chirurgical Observations (1775), Reprinted in National Cancer Inst. Monogr., 1963, 10, 7-13.

5. Cook, J. W.; Hewett, C. L.; Hieger, I. J. Chem. Soc. 1973, 395-405.

6. Evaluation of Carcinogenic Risk; International Agency for Research on Cancer Monographs, 1972; Vol. 3.

7. Chemicals and Human Cancer; International Agency for Research on Cancer Monographs, 1979; Suppl. 1.

8. Chemicals and Industries Associated with Human Cancer; International Agency for Research on Cancer Monographs, 1982; Suppl. 4.

9. Harvey, R. G. In Polycyclic Hydrocarbons and Carcinogenesis; Harvey, R. G., Ed.; American Chemical Society: Washington, D.C., 1984; p. 35.

10. Grasso, P.; O'Hare, C. In Chemical Carcinogens; Searle, C. E., Ed.; American Chemical Society: Washington, D.C., 1976; p. 701.

11. Brown, R. A.; Huffman, H. L. Science 1976, 191, 847-849.

12. Shabad, L. M. J. Natl. Cancer Inst. 1980, 64, 405-410.

13. Maugh, T. H., II. Science 1984, 226, 1183-1184.

14. Miller, E. C. Cancer Res. 1978, 38, 1479-1496.

15. Chemical Carcinogenesis; Nicolini, C., Ed.; Plenum Press: New York, New York, 1982.

16. Dipple, A. In Polycyclic Hydrocarbons and Carcinogenesis; Harvey, R. G., Ed.; American Chemical Society: Washington, D.C., 1984; Chapt. 1.

17. Bresnick, E. In In Vitro Metabolic Activation in Mutagenesis Testing; des Serres, F. J.; Fouts, J. R.; Bend, J. R.; Philpot, R. M., Eds.; North-Holland: New York, New York, 1976; pp. 91-104.

18. Borek, C., Sachs, L. Proc. Natl. Acad. Sci., U.S.A. 1967, 57, 1522-1527.

19. Kakunaga, T. Cancer Res. 1975, 35, 1637-1642.

20. Slater, T. F. Free Radical Mechanisms in Tissue Injury; Pion Limited: London, England, 1972.

21. Cavalieri, E. L.; Rogan, E. G. In Polycyclic Hydrocarbons and Carcinogenesis; Harvey, R. G., Ed.; American Chemical Society: Washington, D.C., 1984; Chapt. 11.

22. Lehr, R. E.; Kumar, S.; Levin, W.; Wood, A. W.; Chang, R. L.; Conney, A. H.; Yagi, H.; Sayer, J. M.; Jerina, D. M. In Polycyclic Hydrocarbons and Carcinogenesis; Harvey, R. G., Ed.; American Chemical Society: Washington, D.C., 1984; Chapt. 4.

23. Grover, P. L. In Biological Carcinogenesis; Rich, M. A.; Furmanski, P., Eds.; Marcel Dekker: New York, New York, 1982; pp. 61-79.

24. Jerina, D. M.; Daly, J. W. In Drug Metabolism - from Microbe to Man; Parke, D. V.; Smith, R. L., Eds.; Taylor and Francis, Ltd.: London, England, 1976; pp. 13-32.

25. Phillips, D. H. Nature 1983, 303, 468-472.

26. Harvey, R. G. American Scientist 1982, 70, 386-393.

27. Dipple, A. Cancer Res. 1983, 43, 2422s-2425s.

28. Conney, A. H. Cancer Res. 1982, 42, 4875-4917.

29. Jerina, D. M.; Lehr, R. E.; Yagi, H.; Hernandez, O.; Dansette, P. M.; Wislocki, P. G.; Wood, A. W.; Chang, R. L.; Levin, W.; Conney, A. H. In In Vitro Metabolic Activation in Mutagenesis Testing; de Serres, F. J.; Fouts, J. R.; Bend, J. R.; Philpot, R. M., Eds.; North-Holland: New York, New York, 1976; pp. 159-177.

30. Jerina, D. M.; Lehr, R. E. In Microsomes and Drug Oxidations; Ulbrick, V.; Roots, I.; Hilderbrandt, A.; Estabrook, R. W., Eds.; Pergamon Press: Elmsford, New York, 1978; pp. 709-720.

31. Jeffrey, A. M. In Polycyclic Hydrocarbons and Carcinogenesis; Harvey, R. G., Ed.; American Chemical Society: Washington, D. C., 1985; Chapt. 8.

32. Rogan, E. G.; Cavalieri, E. L.; Tribbels, S. R.; Cremonesi, P.; Warner, C. D.; Nagel, D. L.; Tomer, K. B.; Cerny, R. L.; Gross, M. L. J. Amer. Chem. Soc. in press.

33. Cavalieri, E.; Calvin, M. Proc. Natl. Acad. Sci. U.S.A. 1971, 68, 1251-1253.

34. Report on DNA adducts workshop measurements subgroup, Oak Ridge National Laboratory, Oak Ridge, Tennessee, 1986.

35. Harris, C. C.; Yolken, R. H.; Hsu, I. C. In Methods in Cancer Research; Busch, H.; Yoeman, L. C., Eds.; Academic Press: New York, New York, 1982; pp. 213-243.

36. Perera, F. P.; Poirier, M. C.; Yuspa, S. H.; Nakayama, J.; Jaretzki, A.; Curnen, M. M.; Knowles, D. M.; Weinstein, I. B. Carcinogenesis 1982, 3, 1405-1410.

37. Hsu, I. C.; Poirier, M. C.; Yuspa, S. H.; Grunberger, D.; Weinstein, I. B.; Yolken, R. H.; Harris, C. C. Cancer Res. 1981, 41, 1091-1095.

38. Santella, R. M.; Lin, C. D.; Cleveland, W. L.; Weinstein, I. B. Carcinogenesis 1984, 5, 373-377.

39. Reddy, M. V.; Gupta, R. C.; Randerath, E.; Randerath, K. Carcinogenesis 1984, 5, 231-243.

40. Gupta, R. C.; Reddy, M. V.; Randerath, K. Carcinogenesis 1982, 3, 1081-1092.

41. Randerath, K.; Randerath, E.; Agrawal, H. P.; Gupta, R. C.; Schurdak, M. E.; Reddy, M. V. Environ. Health Perspect. 1985, 62, 57-65.

42. Randerath, K.; Reddy, M. V.; Gupta, R. C. Proc. Natl. Acad. Sci. 1981, 78, 6126-6129.

43. Reddy, M. V.; Gupta, R. C.; Randerath, K. Anal. Biochem. 1981, 78, 6126-6129.

44. Nazareth, A.; Joppich, M.; Abdel-Baky, S.; O'Connell, K.; Sentissi, A.; Giese, R. W. J. Chromatogr. 1984, 314, 201-210.

45. Mohamed, G. B.; Nazareth, A.; Hayes, M. J.; Giese, R. W.; Vouros, P. J. Chromatogr. 1984, 314, 211-217.

46. Fisher, D. H.; Adams, J.; Giese, R. W. Environ. Health Perspect. 1985, 62, 67-71.

47. Burlingame, A. L.; Straub, K.; Baillie, T. A. Mass Spectrom. Rev. 1983, 2, 331-387.

48. Tomer, K. B.; Gross, M. L.; Deinzer, M. L. Anal. Chem. 1986, 58, 2527-2534.

49. Crow, F. W.; Tomer, K. B.; Gross, M. L.; McCloskey, J. A.; Bergstrom, D. E. Anal. Biochem. 1984, 139, 243-262.

50. Wickramanayake, P. P.; Arbogast, B. L.; Buhler, D. R.; Deinzer, M. L.; Burlingame, A. L. J. Am. Chem. Soc. 1985, 107, 2485-2488.

51. Gross, M. L.; Tomer, K. B.; Cerny, R. L.; Giblin, D. E. In Mass Spectrometry in the Analysis of Large Molecules; McNeal, C. J., Ed.; John Wiley and Sons Ltd.: New York, New York, 1986; pp. 171-190.

52. Vo-Dinh, T.; Martinex, P. R. Anal. Chim. Acta 1981, 125, 13-19.

53. Rahn, R. O.; Chang, S. S.; Holland, J. M.; Stephens, T. J.; Smith, L. H. J. Biochem. Biophys. Methods 1980, 3, 285-291.

54. Vo-Dinh, T.; Gammage, R. B.; Hawthorne, A. R.; Thorngate, J. H. Environ. Sci. Technol. 1978, 12, 1297-1302.

55. Vahakangas, K.; Trivers, G.; Rowe, M.; Harris, C. C. Environ. Health Perspect. 1985, 62, 101-104.

56. Vahakangas, K.; Haugen, A.; Harris, C. C. Carcinogenesis 1985, 6, 1109-1116.

57. Shugart, L.; Holland, J. M.; Rahn, R. O. Carcinogenesis 1983, 4, 195-198.

58. Rahn, R. O.; Chang, S. S.; Holland, J. M.; Shugart, L. R. Biochem. Biophys. Res. Commun. 1982, 109, 262-268.

59. Selkirk, J. K. In Advances in Chromatography; Giddings, J. C.; Gruska, E.; Cazes, J.; Brown, P. R., Eds.; Marcel Dekker: New York, New York, 1978; Vol. 16, pp. 1-36.

60. Shugart, L. Anal. Biochem. 1986, 152, 365-369.

61. Heisig, V.; Jeffrey, A. M.; McGlade, M. J.; Small, G. J. Science 1984, 223, 289-291.

62. Personov, R. I. In Spectroscopy and Excitation of Condensed Molecular Systems; Agranovich, V. M.; Hochstrasser, R. M., Eds.; North-Holland: New York, New York, 1983; pp. 555-619.

63. Brown, J. C.; Edelson, M. C.; Small, G. J. Anal. Chem. 1978, 50, 1394-1397.

64. Brown, J. C.; Hayes, J. M.; Warren, J. A.; Small, G. J. In Lasers in Chemical Analysis; Hieftje, G. M.; Travis, J. C.; Lytle, F. E., Eds.; Humana Press, Inc.: Clifton, New Jersey, 1981; Chapt. 12.

65. Kohler, B. E. In Chemical and Biochemical Applications of Lasers; Moore, C. B., Ed.; Academic Press: New York, New York, 1979; Vol. 4, pp. 31-53.

66. Brown, J. C. Ph.D. Dissertation, Iowa State University, Ames, Iowa, 1982.

67. Brown, H. S.; Jeffrey, A. M.; Weinstein, I. B. Cancer Res. 1979, 39, 1673-1677.

68. Wallin, H.; Jeffrey, A. M.; Santella, R. M. Cancer Lett. 1987, 35, 139-146.

69. McGlade, M. J. Master's Thesis, Iowa State University, Ames, Iowa, 1983.

70. Sanders, M. J.; Cooper, R. S.; Small, G. J.; Heisig, V.; Jeffrey, A. M. Anal. Chem. 1985, 57, 1148-1152.

71. Harris, J. M.; Lytle, F. E.; McCain, T. C. Anal. Chem. 1976, 48, 2095-2098.

72. Chiang, I.; Hayes, J. M.; Small, G. J. Anal. Chem. 1982, 54, 315-318.

73. Brown, J. C.; Duncanson, J. A., Jr.; Small, G. J. Anal. Chem. 1980, 52, 1711-1715.

74. Sanders, M. J.; Cooper, R. S.; Jankowiak, R.; Small, G. J.; Heisig, V.; Jeffrey, A. M. Anal. Chem. 1986, 58, 816-820.

75. Jankowiak, R.; Cooper, R. S.; Zamzow, D.; Small, G. J.; Doskocil, G.; Jeffrey, A. M. Research in Chemical Toxicology 1987, submitted for publication.

76. Burland, D. M.; Haarer, D. IBM J. Res. Develop. 1979, 23, 534-546.

77. Friedrich, J.; Haarer, D. Angew. Chem. Int. Ed. Eng. 1984, 23, 113-140.

78. Hoffman, D.; Bondinell, W. E.; Wynder, E. L. Science 1974, 183, 215-216.

79. Hecht, S. S.; Bondinell, W. E.; Hoffman, D. J. J. Natl. Cancer Inst. 1974, 53, 1121-1133.

80. Warren, J. A.; Hayes, J. M.; Small, G. J. Chem. Phys. 1986, 102, 313-323.

81. Birks, J. B. Photophysics of Aromatic Molecules; Wiley-Interscience: New York, New York, 1970.

82. Weber, M. J., Ed. J. Lum. 1987, 36, Nos. 4 and 5.

83. Hayes, J. M.; Jankowiak, R.; Small, G. J. In Topics in Current Physics, Persistent Spectral Hole Burning: Science and Applications; Moerner, W. E., Ed.; Springer-Verlag: New York, New York, 1987; Chapt. 5 and other chapters therein.

84. Jankowiak, R.; Small, G. J. Science 1987, 237, 618-625.

85. Jankowiak, R.; Shu, L.; Kenney, M. J.; Small, G. J. J. Lum. 1987, 36, 293-305.

86. Walsh, C. A.; Berg, M.; Narashimhan, L. R.; Fayer, M. D. Chem. Phys. Lett. 1986, 130, 6-11.

87. Walsh, C. A.; Berg, M.; Narashimhan, L. R.; Fayer, M. D. J. Chem. Phys. 1987, 86, 77-87.

88. Personov, R. I.; Al'shits, E. I.; Bykovskaya, L. A. Opt. Commun. 1972, 6, 169-173.

89. Stillinger, F. H. Science 1984, 225, 983-989.

90. Hayes, J. M.; Small, G. J. Chem. Phys. 1978, 27, 151-157.

91. Kharlamov, B. M.; Personov, R. I.; Bykovskaya, L. A. Opt. Commun. 1974, 12, 191-193.

92. Bogner, U.; Schwarz, R. Phys. Rev. 1981, B24, 2846-2849.

93. Fünfschilling, J.; Glatz, D.; Zschokke-Grenacher, I. J. Lum. 1986, 36, 85-92.

94. Osterman-Golkar, S.; Ehrenberg, L.; Segerback, D.; Halstrom, I. Mutat. Res. 1976, 34, 1-10.

95. Koloczek, H.; Fidy, J.; Vanderkooi, J. M. Submitted to J. Chem. Phys. for publication.

96. Avarmaa, R.; Renge, I.; Mauring, K. FEBS Lett. 1984, 167, 186-190.

97. Harvey, R. G. In Polycyclic Hydrocarbons and Carcinogenesis; Harvey, R. G., Ed.; American Chemical Society: Washington, D.C., 1985, p. viii.

98. Essigmann, J. M.; Croy, R. G.; Bennett, R. A.; Wogan, G. N. In Chemical Carcinogenesis; Nicolini, C., Ed.; Plenum Press: New York, New York, 1982; pp. 47-66.

VI. ACKNOWLEDGMENTS

It is a pleasure to acknowledge and thank all of the people who supported me during my stay at Iowa State University. This research was funded by the Office of Health and Environmental Research, Office of Energy Research.

I would like to express my sincere thanks and gratitude to my research advisor, Dr. Gerald J. Small, for all of his help and guidance during the course of this research. I would also like to thank him for his flattering introduction before my final oral examination, even though he failed to mention that my undergraduate arm wrestling scholarship was a "full-ride" scholarship.

I would like to acknowledge and thank Dr. John M. Hayes for all of his help and advice in the laboratory. I am also grateful for his informative discussions on the theoretical aspects of this research. A thank you also for taking the time to proofread this dissertation.

I would like to thank the members of Dr. Small's research group, particularly Dr. Matthew J. Sanders, Dr. Ryszard Jankowiak, and Dan Zamzow for their extensive help and advice during this research. I would also like to thank Dr. Thomas Carter, Dr. Bryan L. Fearey, Bryan Isaac, Mike Kenney, Kevin Gillie, Steve Johnson, and Kyuseok Song for their support and friendship. Thank you also for the

entertaining pranks, even though the incident with the urine sample tube shortened my lifespan considerably.

An acknowledgment and thank you to Dr. Alan M. Jeffrey, Dr. Ercole Cavalieri, and Dr. Elanore Rogan for providing the samples for this research.

A special thank you to the friends I have come to know while in Ames, particularly Mark and Susan Havener-Goodyear and the family of Jerry and Judy Smith.

A very special thank you to my mother, Thelma Cooper, and late father, Richard A. Cooper, along with my brothers for their love, support, encouragement, and especially for their fine example which has helped me throughout my life.

Finally, my love and thanks to my fiancee, Linda Warth, for her patience, support, and encouragement. I would especially like to thank her for all of the joyful moments we have spent together.